MNRAS 000, 1–16 (2018) Preprint 15 October 2018 Compiled using MNRAS LATEX style file v3.0

Morphological evolution and galactic sizes in the L-Galaxies SA model

Dimitrios Irodotou[1]★, Peter A. Thomas[1], Bruno M. Henriques[2], Mark T. Sargent[1]
[1]Astronomy Centre, University of Sussex, Falmer, Brighton BN1 9QH, UK
[2]Institute for Astronomy, Department of Physics, ETH Zurich, 8093 Zurich, Switzerland

Draft - 15 October 2018

ABSTRACT

In this work we update the L-Galaxies semi-analytic model (SAM) to better follow the physical processes responsible for the growth of bulges via disk instabilities (leading to pseudo-bulges) and mergers (leading to classical bulges), showing the impact of these processes on the fractional breakdown of our galaxies into different morphological types, and obtaining an excellent fit to the morphology-mass relation. We find that an accurate match to the observed correlation between stellar disk scale length and mass at $z \sim 0.0$ requires that the gas loses 20% of its initial specific angular momentum to the corresponding dark matter halo during the formation of the cold gas disk. With this assumption, we reproduce the observed trends between the stellar mass and specific angular momentum for both disk- and bulge-dominated galaxies, with late-type galaxies rotating faster than early-types of the same mass. We include dissipation of energy in gas-rich mergers, thus reducing the merger remnant sizes, which allows us to match the observed mass-size relation for bulge-dominated systems. Finally, we present the baryonic Tully-Fisher relation for gas- and disk-dominated galaxies, and find that our trend agrees well with the present-day observational constraints.

Key words: galaxies: formation – galaxies: evolution – galaxies: bulges – methods: analytical

1 INTRODUCTION

In the widely accepted Lambda Cold Dark Matter (ΛCDM) scenario the baryonic matter collapses into the centres of dark matter haloes, where it forms rotationally supported disks (Fall & Efstathiou 1980; Blumenthal et al. 1984; Peebles 1984). Initially, the dark matter haloes acquire their angular momentum through tidal interactions (Peebles 1969; White 1984; Barnes & Efstathiou 1987), and the associated gas disks are assumed to obtain the same specific angular momentum. Eventually, the collapsed gas will form stars and subsequently galaxies (White & Rees 1978). While these dark matter structures evolve over time, they grow in mass and size through accretion and/or repeated mergers (Lacey & Cole 1993). These phenomena are expected to affect the environment in which each galaxy resides, hence produce galaxies characterised by a plethora of different properties.

Much of the current knowledge on galaxy formation and evolution is acquired through studying scaling relations of galactic structural and kinematic properties (e.g., Faber & Jackson 1976; Djorgovski & Davis 1987; Kormendy 1977). On that account, in this work we reproduce the observed relations in order to investigate the impact of the implemented bulge growth and disk instability models on galactic sizes and morphologies.

The impending section is designed to present a detailed overview of the hierarchical framework of galaxy formation and demonstrate how pioneering theories along with simulations and observational surveys attempt to piece together the puzzle of galaxy formation and evolution.

1.1 The angular momentum of baryons

As noted by Cole et al. (2000), the assumption that baryons conserve their specific angular momentum when cooling to form luminous galaxies is not a trivial one (see also Mo et al. 1998, for a discussion on this topic). A few seminal theoretical works and simulations (e.g., Blumenthal et al. 1986; Flores et al. 1993) detected an interaction between the dark and the baryonic matter when studied the gravitational pulling in of the dark matter during the contraction of the dissipative disk material. In fact, during disk formation the rotation curve is altered both through disk gravitational effects and

★ E-mail: Dimitrios.Irodotou@sussex.ac.uk

through the contraction it induces in the innermost parts of the dark matter halo.

In addition, numerical hydrodynamical simulations of that era (e.g., Navarro & White 1993, 1994; Navarro et al. 1995; Navarro & Steinmetz 1997) found that cold gas loses most of its angular momentum to the dark matter halo via dynamical friction. Navarro & Steinmetz (2000) came to the same conclusion when they tried to derive a lower limit to the mass of the halo that encapsulates our Galaxy. Furthermore, Katz & Gunn (1991) used the TREESPH code of Hernquist & Katz (1989) and simulated the collapse of isolated systems containing dark and baryonic (gas) matter in a 10 to 1 ratio. They found that during the disk formation process most of the gas ended up in a cold, rotationally-supported disk and while the gas was settling into this disk it was transferring angular momentum to the dark halo. Their results suggested that the gas disk loses between 48 and 73 percent of its original angular momentum mainly due to gravitational interaction between the gas and the dark matter as the clumps spiral together and merge.

A "second generation" of numerical simulations (e.g., Kaufmann et al. 2007; Zavala et al. 2008) also concluded that baryons transfer a fraction of their angular momentum to dark matter via gravitational torques, hence galaxy formation spins up the halo within $0.1R_{\rm vir}$ (Bett et al. 2010). As discussed by Kimm et al. (2011), in the standard picture of galaxy formation the angular momentum of the gas becomes distinctively different from that of the dark matter. In addition, the modulus of the specific angular momentum inside the virial sphere is not conserved neither for the dark matter nor for the gas, due to the misalignment between the angular momentum of newly accreted material and that of the whole halo. Furthermore, Danovich et al. (2015) used the hydro-gravitational code ART (Kravtsov 2003) and analysed the acquisition of angular momentum of the baryonic and dark matter by separating the infall process into 4 different phases. They identified angular momentum losses in phase III (inner halo) and concluded that the angular momentum is not conserved, since it is transferred by torques to the rest of the gas, stars and dark matter. More recently, Stevens et al. (2017) investigated if the angular momentum of gas particles that cool thought the hot mode down onto galaxies is conserved. They studied both the 'strong' and the 'weak' angular momentum conservation scenario (Fall 2002) and concluded that gas in EAGLE galaxies loses approximately 60 percent of its specific angular momentum over the course of cooling.

Given the above results and provided that the cold gas is being feed to the majority of galaxies through thin and dense filaments that penetrate deep inside the virial radius of their host halo (e.g., Kereš et al. 2005; Ocvirk et al. 2008; Dekel et al. 2009), the standard galaxy formation framework and the validity of its assumptions seem to require a reassessment. Hence, even though modelling explicitly these processes in semi-analytic models remains a challenging task, in this work we attempt to include this phenomenon (i.e., angular momentum losses during cooling) in the L-Galaxies model [1] (see Section 2.1) and investigate its direct impact on scaling relations between galactic properties (see Section 3 and Appendix A.).

[1] http://galformod.mpa-garching.mpg.de/public/LGalaxies/

1.2 Mergers and disk instabilities

In the hierarchical picture of structure formation, galaxy mergers have the ability to redesign the morphology of the progenitors (Toomre & Toomre 1972; Barnes & Hernquist 1996; Hopkins et al. 2010b). In particular, major mergers (Kauffmann et al. 1993; Baugh et al. 1996), multiple minor mergers (Bournaud et al. 2007) and satellite mergers (Aguerri et al. 2001) are considered to be the natural culprits for converting the stellar orbits from circular to random, hence forming spheroid-like components (i.e., classical bulges) and dispersion-supported galaxies.

In addition to mergers, internal secular processes (see Sellwood 2014, for a review), such as buckling instability of bars, (Combes et al. 1990; Raha et al. 1991; Martinez-Valpuesta et al. 2006) are able to trigger disk instabilities (Toomre 1964; Efstathiou et al. 1982) and, in some cases, funnel gas to the centre of the galaxy (Combes & Sanders 1981; Pfenniger & Norman 1990; Englmaier & Shlosman 2004), thus enhancing central star formation (Hawarden et al. 1986; Friedli & Benz 1995; Jogee 2006; Holmes et al. 2015). In specific cases (Hopkins et al. 2009a; Stewart et al. 2009; Governato et al. 2009; Guedes et al. 2013) mergers may as well constitute a mechanism able to trigger disk instabilities and create inner disk structures (Eliche-Moral et al. 2006, 2011) or starbust activity (Mihos & Hernquist 1994). In order for a disk to regain its dynamical equilibrium, it has to rearrange its mass distribution by transferring a sufficient amount of mass inwards. This mechanism will culminate in the formation of a component called pseudo-bulge (see Kormendy & Kennicutt 2004, and references therein).

Works carried out by several authors (e.g., Jog & Solomon 1984a,b; Bertin & Romeo 1988) suggest that both stellar and gaseous disks contribute to the stability of the galactic disk and that the instability criterion (see Equation 6) should be adjusted in order to include both components (Jog 1996; Elmegreen 1995).

As a result, Goz et al. (2014) used the GADGET-3 code (Springel 2005) and concluded that the time a bar instability occurs is linked to the time a two-component disk becomes unstable. In addition, Ghosh & Jog (2015) had to treat the galactic disk as a two-component system in order to explain the long-lived two-armed spiral pattern in galaxies. In conjunction with these, Goldbaum et al. (2016) used the Enzo AMR hydrodynamics code (Bryan et al. 2014) and argued that inflowing unstable gas could be responsible for the star formation activity in the inner parts of a galactic disk, since it may be sufficient enough to counterbalance the star formation that is suppressed by its feedback. Romeo & Fathi (2016) came to the same conclusion when they studied the starburst activity of a particular galaxy.

It is thus clear that various theoretical and/or observational studies had to analyse galactic disks instabilities based on this approach in order to explain the observed behaviours. This dictates that modelling attempts should also follow the same path (see Section 2.2 for further discussion).

1.3 Bulges: classical and pseudo

Numerous authors attempted to investigate whether the aforementioned bulge formation scenarios lead to different bulge types with distinct intrinsic properties. Therefore, a plethora of studies utilised various physical quantities that can be observationally constrained (e.g., Fisher & Drory 2016), in order to elucidate this dichotomy.

Although some studies (e.g., Athanassoula 2005; Sachdeva & Saha 2018) divide bulges into more categories, most authors distinguish two major types: pseudo and classical. In fact, Andredakis & Sanders (1994); Andredakis et al. (1995); Carollo (1999) and more recently Scarlata et al. (2004) studied early- and intermediate-type spiral galaxies and concluded that bulges fall into two categories: those that can be described by an exponential profile and those by an $r^{1/4}$ profile. Moreover, Courteau et al. (1996) used a bulge-to-disk decomposition to calculate the ratio between bulge and disk scale lengths and concluded that their observations (correlated B/D scale lengths) strongly support a secular evolution model in which bulges with exponential surface brightness profiles emerge via disk instabilities. A few years later, MacArthur et al. (2003) not only confirmed but also reinforced these results. Additionally, Fisher (2006); Fisher et al. (2009) compared the profile of star formation in pseudo- and classical bulges and concluded that their stars are formed via different mechanisms. Furthermore, Fisher & Drory (2008) analysed the Sérsic index of pseudo- and classical bulges and found that 90% of the former have $n_{\rm b} < 2$ and all of the latter $n_{\rm b} > 2$. In addition, Ho (2008) found that black holes live inside both pseudo- and classical bulges, but while Kormendy & Ho (2013) observationally established that their mass is tightly related to the stellar mass and velocity dispersion of classical bulges, Kormendy et al. (2011) concluded that this behaviour does not appear to be true for pseudo-bulges. Finally, Fabricius et al. (2012) observed a correlation between the shape of the velocity dispersion profile and the bulge type and concluded that classical bulges have centrally peaked and higher velocity dispersion profiles than pseudo-bulges.

It becomes apparent that there is a lot of evidence suggesting that this dichotomy can reveal a diversity in bulge properties. This motivated us to revise the disk instability recipe in the L-Galaxies model (see Section 2.2) and investigate these two distinct bulge types (see Section 2.3).

1.4 Previous modelling work and the existing L-Galaxies model

The majority of the "first generation" (e.g., White & Frenk 1991; Cole et al. 1994; Baugh et al. 1996; Kauffmann et al. 1999; Somerville & Primack 1999; Kauffmann & Haehnelt 2000; Cole et al. 2000; Springel et al. 2005; Croton et al. 2006) of pioneering analytic and semi-analytic models of galaxy formation followed Fall & Efstathiou (1980) and Mo et al. (1998) and computed disk sizes based on the assumptions that a) the cold gas disk inherits the specific angular momentum of the dark matter halo in which it forms, and b) the gas conserves its angular momentum while cooling (e.g., Cole et al. 1994; Dalcanton et al. 1997; Mo et al. 1998). The fact that these early studies were able to match fundamental observed relations, such as the Tully-Fisher, encouraged all the forthcoming semi-analytic galaxy formation models to rely on these assumptions (e.g., Cole et al. 2000; Hatton et al. 2003; Monaco et al. 2007; Somerville et al. 2008; Dutton & van den Bosch 2009; Guo et al. 2011; Tonini et al. 2016). However, the degree to which the formation and growth of galaxies is affected by the aforesaid assumptions remains a subject under investigation which necessitate a more precise treatment, as discussed in Section 2.1, below.

As presented above, gaseous disks have an influential role in galactic dynamics which becomes apparent when one considers their contribution to disk stability. Despite the rich literature, most past modelling works (e.g., De Lucia & Blaizot 2007; Monaco et al. 2007; Somerville et al. 2008; Benson 2012; Henriques et al. 2013; Gonzalez-Perez et al. 2014; Gargiulo et al. 2015; Croton et al. 2016) have relied on a one-component stability parameter. Opposed to them, Tonini et al. (2016) released the SAGE (Semi-Analytic Galaxy Evolution) model in which their new disk instability recipe treats the galactic disk as a stellar+gaseous disk with a mass-averaged scale length. They check the stability of this composite disk and transfer inwards, in proportion, an adequate amount of stars and gas.

The most recent version of the L-Galaxies model (Henriques et al. 2015, hereafter HWT15) invokes a simple argument to address the stellar disk instability and identify the stellar mass that has to be put into the bulge. It only takes into account the stability of the stellar disk and, as a consequence, underestimates disk instabilities and fails to reproduce the observed morphological fraction of galaxies (see Section 3.3). Furthermore, the half-mass radius of classical bulges is calculated via energy conservation and the virial theorem, as described in Guo et al. (2011). This approach overestimates the size of bulges, which can be remedied by considering dissipation during gas-rich mergers (see Sections 2.3.1 and 3.6.2).

1.5 Outline of the paper

This paper is organised as follows. In Section 2 we briefly describe a few vital processes regarding the L-Galaxies model's approach to simulate the formation and evolution of galaxies. In addition, we present the new merger remnant size and disk instability recipes we included in our model. Section 3 contains our results and the conclusions are shown in Section 4.

2 THE MODEL

The L-Galaxies semi-analytic model has been well-described in the literature and we refer the reader to HWT15 for more details. Here, we briefly explain some key processes that are relevant to the purpose of this study and introduce: angular momentum losses during cooling and the updated disk instability and merger remnant size recipes.

2.1 Formation and properties of the gaseous and stellar disks

In general, the L-Galaxies SAM can be applied to the dark matter merger trees produced by the Millennium (Springel et al. 2005) and Millennium-II (Boylan-Kolchin et al. 2009)

simulations. However, in this paper we use merger trees produced by the former in order to derive galactic properties. As haloes form and grow, they are assigned a cosmic abundance of diffuse primordial gas, which is assumed to be shock-heated to the virial temperature (Rees & Ostriker 1977; Silk 1977; White & Rees 1978). That gas will either cool immediately and be added to the cold gas disk of the central galaxy, or form a quasi-static hot atmosphere and accrete onto the disk at a slower pace (see Section S1.4 of HWT15).

Hitherto the L-Galaxies model followed the two core assumptions of Fall & Efstathiou (1980), namely: a) baryons and dark matter acquire identical specific angular momentum distributions and b) the former conserve their angular momentum while cooling. In this work, we account for the angular momentum losses discussed in Section 1.1 by assuming that the initial specific angular momentum of the cold gas is a fraction $f = 0.8$ of the specific angular momentum of the halo within which it is embedded. This factor is somewhat arbitrary but has been chosen to approximately match the galactic morphologies and sizes, as discussed in Section 3.3, Section 3.6 and Appendix A. We note that the angular momentum loss should be transmitted to the dark matter but this effect will be relatively small and we choose to neglect it.

We track the angular momentum of both the gaseous and stellar disks using the method introduced by Guo et al. (2011). Both are assumed to be infinitesimally thin, in centrifugal equilibrium within an isothermal potential, and to have exponential surface density profiles:

$$\Sigma(R) = \Sigma_0 \exp(-R/R_\mathrm{d}) \,, \tag{1}$$

where $\Sigma_0 = M_\mathrm{d}/2\pi {R_\mathrm{d}}^2$ is the central surface density and M_d and R_d are the corresponding (total) disk mass and scale length, respectively. The latter two are related via:

$$R_\mathrm{d} = \frac{J}{2M_\mathrm{d} \cdot V_\mathrm{c}} \,, \tag{2}$$

where J is the angular momentum and V_c is the circular velocity of the isothermal halo.

Quiescent star formation occurs in regions where the gas exceeds a critical value surface density. The star formation rate is given by:

$$\dot{M}_\star = \alpha_\mathrm{SF} \frac{M_\mathrm{d,gas} - M_\mathrm{crit}}{t_\mathrm{dyn}} \,, \tag{3}$$

where α_SF is the star formation efficiency, $M_\mathrm{d,gas}$ is the total mass of cold gas, $t_\mathrm{dyn} = 3R_\mathrm{d}/V_\mathrm{c}$ is the characteristic timescale at the edge of the star-forming disk and M_crit is a threshold mass (Kauffmann et al. 1999) given by:

$$M_\mathrm{crit} = M_\mathrm{crit,0} \left(\frac{V_\mathrm{c}}{200\,\mathrm{km\,s^{-1}}} \right) \left(\frac{R_\mathrm{d,gas}}{10\,\mathrm{kpc}} \right) \,, \tag{4}$$

where $M_\mathrm{crit,0}$ is a fixed constant, V_c is the circular velocity of the isothermal halo and $R_\mathrm{d,gas}$ the gas disk scale length. Note that both $\alpha_\mathrm{SF} = 0.025$ and $M_\mathrm{crit,0} = 0.24 \cdot 10^{10}\,\mathrm{M_\odot}$ were free parameters in the MCMC sampling of HWT15 – see their Table S1.

As discussed in Guo et al. (2011), there are three mechanisms capable of altering the angular momentum vector of the gaseous disk, namely the addition of gas by cooling, the removal of gas through star formation and the accretion from minor mergers. These can be expressed mathematically by the following formula:

$$\begin{aligned} \Delta\vec{J}_\mathrm{gas} &= \delta\vec{J}_\mathrm{gas,cooling} + \delta\vec{J}_\mathrm{gas,SF} + \delta\vec{J}_\mathrm{gas,acc.} \\ &= f\frac{\vec{J}_\mathrm{DM}}{M_\mathrm{DM}}\dot{M}_\mathrm{cool} \cdot \delta t \\ &- \frac{\vec{J}_\mathrm{gas}}{M_\mathrm{d,gas}}((1-R_\mathrm{ret})\dot{M}_\star \cdot \delta t + \delta M_\mathrm{reheat}) \\ &+ \frac{\vec{J}_\mathrm{DM}}{M_\mathrm{DM}} M_\mathrm{gas,sat} \,, \end{aligned} \tag{5}$$

where the factor $f = 0.8$ accounts for angular momentum losses during cooling, $\dot{M}_\mathrm{cool}$ is the cooling rate (see Eq. S6 and S7 of HWT15), δt is the time interval, $(1-R_\mathrm{ret})\dot{M}_\star$ is the formation rate of long lived stars (see Eq. S14 of HWT15), δM_reheat is the cold gas reheated into the hot atmosphere as a result of star formation activity (see Eq. S18 of HWT15) and $M_\mathrm{gas,sat}$ is the cold gas mass of the merging satellites.

Each star formation episode gives rise to associated feedback of energy, reheating some disk material and possibly expelling gas from the halo; for a detailed review of those processes in the L-Galaxies SAM we refer the reader to Sections S1.7 to S1.9 of HWT15.

2.2 Disk instabilities

In our updated instability recipe we treat galactic disks as "two-component" systems where the stability of each disk (i.e., stellar or gaseous) is checked independently. We adopt the simple criterion from Mo et al. (1998):

$$\epsilon \equiv \frac{V_\mathrm{c}}{(GM_\mathrm{d}/R_\mathrm{d})^{1/2}} \,, \tag{6}$$

where V_c is the rotational velocity which for both disks is approximated by the circular velocity of their host halo and M_d and R_d is the mass and scale length of either the stellar ($M_\mathrm{d,\star}$) or the gaseous ($M_\mathrm{d,gas}$) disk. When $\epsilon < \epsilon_\mathrm{disk}$ the self-gravity of the disk is dominant and the disk becomes unstable. Even though the onset of the disk instability has been found to be characterised by the inequality $\epsilon \leq 1.1$ for stellar (Efstathiou et al. 1982) and $\epsilon \leq 0.9$ for gaseous disks (Christodoulou et al. 1995); in this work we adopt $\epsilon_\mathrm{disk} = 1$ for both disks since this value lies within the limits (ranging from 0.8 to 1.2) provided by Mo et al. (1998).

We begin by utilising the above criterion and investigating the stability of the gaseous disk. When the attraction due to self-gravity (represented by $M_\mathrm{d,gas}$) overcomes the centrifugal force due to rotation (represented by V_c) the disk is termed unstable. We assume that the unstable cold gas triggers two mechanisms: a quasar mode in which we transfer a percentage of the unstable cold gas to the central black hole, and a burst of star formation in which the remaining unstable cold gas is consumed as a fuel. We simulate the former by invoking a modified version of the quasar mode Eq. S23 of HWT15:

$$\Delta M_\mathrm{BH,Q} = \frac{f_\mathrm{BH}}{1 + (V_\mathrm{BH}/V_\mathrm{200c})^2} M_\mathrm{gas,unstable} \,, \tag{7}$$

where $f_\mathrm{BH} = 0.041$ and $V_\mathrm{BH} = 750\,\mathrm{km\,s^{-1}}$ are two adjustable parameters which control the fraction of the available cold gas that is accreted and the virial velocity at which the efficiency saturates (see Table S1 of HWT15) and $M_\mathrm{gas,unstable}$ is

the unstable cold gas mass. The remaining unstable cold gas is converted into stars that are left in the stellar disk. Then we invoke again Equation 6 but this time we apply it to the stellar disk. If the stellar disk was, or has become, too massive for its rotational velocity it has to regain its dynamical equilibrium by rearranging its mass distribution. We assume that the excess stellar mass ($M_{\star,\mathrm{unstable}}$) sinks from the innermost part of the stellar disk towards the galactic centre and forms a pseudo-bulge.

The above described disk instability approach is in agreement with several studies which utilised an effective stability parameter and tried to predict whether the local stability is dominated by the stellar or the gaseous disk. Hoffmann & Romeo (2012) found that for $R \leq 0.43 \cdot R_{25}$ (where R_{25} is the B-band isophotal radius at 25 mag arcsec^2) 56% of their galaxies lie in the unstable regime because their gas content drive their effective stability parameter below 1. Surprisingly, Cacciato et al. (2012) found that gas may regulate the two-component stability factor even for disks that are star-dominated. In addition, Romeo & Falstad (2013) used the first three-component analysis of THINGS spirals to conclude that gas (H_2 in particular) plays a dominant role in the stability of the inner parts of a disk, while stars determine its stability at larger distances. More recently, Krumholz et al. (2018) stated that gas, due to its dissipational properties (Elmegreen 2011) and lower velocity dispersion, tends to be the most unstable component especially in gas-rich galaxies (e.g., high-redshift star-forming galaxies and local dwarfs and low-mass spirals).

Finally, we have to note that in the L-Galaxies model these processes take place in systems where the angular momentum of the transferred material is assumed to be negligible and the disk's total angular momentum is conserved. Hence, every action that affects the mass of a disk (either the stellar or the gaseous) will also alter the specific angular momentum of that disk. In particular, processes that decrease (increase) the disk mass will lead into an increase (decrease) in the specific angular momentum, which will cause the disk radius to increase (decrease) in order to counterbalance the mass deviation. In general, an isolated system with constant angular momentum will try to minimise its total energy, and for a self-gravitating disk with negative specific heat it is energetically favourable to expand (Lynden-Bell & Kalnajs 1972; Lynden-Bell & Pringle 1974). Galactic disks are rotationally supported systems, that is to say that their evolution is governed by angular momentum transport. During instabilities angular momentum is transferred outwards as a response to inwards mass movement. Hence, while the inner parts of the disk grow denser, the outer parts expand and become more diffuse.

2.3 Formation and properties of classical and pseudo-bulges

In the L-Galaxies model bulges form through three distinct mechanisms: major mergers, minor mergers and disk instabilities. Major and minor mergers are assumed to produce classical bulges, while disk instabilities lead to the formation of pseudo-bulges.

2.3.1 Classical bulges

Whenever two or more dark matter subhaloes merge, so do their associated galaxies but on a longer timescale determined by 2-body relaxation. In our model we characterise as central galaxies those that dwell in the potential minimum of the most massive subhaloes (hereafter the main halo) and as satellite galaxies those that reside inside the non-dominant subhaloes that are bound to the main halo. The dynamical friction experienced by a satellite galaxy, as it spirals into the central one, will define the time it needs to merge with the central object, and this time is calculated by using the Binney & Tremaine (1987) formula:

$$t_{\mathrm{friction}} = \alpha_{\mathrm{friction}} \frac{V_{\mathrm{200c}} \cdot r_{\mathrm{sat}}^2}{G \cdot M_{\mathrm{sat}} \cdot \ln \Lambda} , \quad (8)$$

where $\alpha_{\mathrm{friction}}$ is a parameter originally set by De Lucia & Blaizot (2007) to match the bright end of the z=0 luminosity functions, V_{200c} is the virial velocity of the main halo, r_{sat} is the distance between the satellite and the central galaxy, M_{sat} is the baryonic mass of the galaxy plus the dark mass of the subhalo and $\ln \Lambda = \ln(1 + M_{\mathrm{200c}}/M_{\mathrm{sat}})$ is the Coulomb logarithm, where M_{halo} is the mass of the main halo.[2]

We distinguish a major from a minor merger based on the ratio of the total baryonic mass (stars+gas), M_1 and M_2, of the satellite and central galaxy, respectively. In major mergers ($M_1/M_2 > 0.1$) the disks of the progenitors are dismantled and both the pre-existing stars and those formed during the merger become part of the resulting bulge-dominated galaxy. In minor mergers, the bulge of the descendant accretes all the stars of the less massive progenitor, while stars formed during this process remain in the remnant's disk. The mass of those stars is calculated by using the "collisional starburst" formulation of Somerville et al. (2000):

$$M_{\star,\mathrm{burst}} = \alpha_{\mathrm{SF,burst}} \left(\frac{M_1}{M_2} \right)^{\beta_{\mathrm{SF,burst}}} M_{\mathrm{d,gas}} , \quad (9)$$

where $\alpha_{\mathrm{SF,burst}}$ and $\beta_{\mathrm{SF,burst}}$ are free parameters and $M_{\mathrm{d,gas}}$ is the total gas disk mass of both galaxies combined.

Galaxy mergers are considered to play a fundamental role in the production of elliptical galaxies, hence having a model able to evaluate the size of the remnant and reproduce its scaling relations across cosmic time is crucial. The HWT15 version of the model calculated the half-mass radius of the remnant using energy conservation arguments, where the final binding energy was equated to the self-binding energies of the two progenitors plus their orbital energy (see Eq. S34 of HWT15). Several authors have argued that this simple picture leads to unrealistic sizes, especially at the low-mass end (Covington et al. 2008; Hopkins et al. 2009b; Shankar et al. 2010; Hopkins et al. 2010a; Covington et al. 2011; Shankar et al. 2013; Porter et al. 2014). This problem mainly arises from the fact that the above approximation does not take into account gas dissipation during mergers, where gas clouds collide and radiate away their kinetic energies. In cases where the gas makes up a significant fraction of the total mass of the progenitors this phenomenon would

[2] Here defined to be the mass within a sphere enclosing a mean density equal to 200 times the critical density.

result in smaller and denser remnants. We follow Covington et al. (2008, 2011) and Tonini et al. (2016) and include a term to account for radiative losses. In this picture the energy conservation formula is given by:

$$E_{\rm final} = E_{\rm initial} + E_{\rm orbital} + E_{\rm radiative}\,, \tag{10}$$

where for major mergers each energy term can be explicitly written as:

$$E_{\rm final} = G\left[\frac{(M_{\star,1} + M_{\star,2} + M_{\star,\rm burst})^2}{R_{\rm final}}\right], \tag{11}$$

$$E_{\rm initial} = G\left(\frac{M_1^2}{R_1} + \frac{M_2^2}{R_2}\right), \tag{12}$$

$$E_{\rm orbital} = G\left(\frac{M_1 \cdot M_2}{R_1 + R_2}\right), \tag{13}$$

$$E_{\rm radiative} = C_{\rm rad} \cdot E_{\rm initial}\left(\frac{M_{\rm gas,1} + M_{\rm gas,2}}{M_1 + M_2}\right), \tag{14}$$

where $M_{\star,\rm i}$, $M_{\rm i}$, $M_{\rm gas,i}$ and $R_{\rm i}$ are the total stellar mass (disk+bulge), total baryonic mass (stars+gas), gas mass and stellar half-mass radius of the i progenitor, $R_{\rm final}$ is the stellar half-mass radius of the remnant, $C_{\rm rad}$ is a parameter which defines the efficiency of the radiative process (see discussion below) and $M_{\star,\rm burst}$ is the mass of the new stars formed during the merger which is given by Equation 9.

For minor mergers we follow Guo et al. (2011) and assume that the total stellar mass of the satellite galaxy is merged with the bulge of the central galaxy, therefore:

$$E_{\rm final} = G\left[\frac{(M_{\rm b,1} + M_{\star,2})^2}{R_{\rm final}}\right], \tag{15}$$

$$E_{\rm initial} = G\left(\frac{M_{\rm b,1}^2}{R_{\rm b,1}} + \frac{M_{\star,2}^2}{R_2}\right), \tag{16}$$

$$E_{\rm orbital} = G\left(\frac{M_{\rm b,1} \cdot M_{\star,2}}{R_{\rm b,1} + R_2}\right) \tag{17}$$

$$E_{\rm radiative} = C_{\rm rad} \cdot E_{\rm initial}\left(\frac{M_{\rm gas,1} + M_{\rm gas,2}}{M_1 + M_2}\right), \tag{18}$$

where $M_{\rm b,1}$ and $R_{\rm b,1}$ are the stellar mass and half-mass radius of the bulge of the more massive progenitor and $M_{\star,2}$ and R_2 are the total stellar mass and half-mass radius of the minor progenitor. Equation 10 indicates that galaxies with higher gas fractions will experience more dissipation during mergers, and since lower mass galaxies have low-mass progenitors which have higher cold gas fractions at all redshifts, the early-wet mergers will produce more compact remnants than late-dry mergers (e.g., Robertson et al. 2006b,a; Dekel & Cox 2006).

Covington et al. (2008) calibrated their model using the N-Body/SPH code GADGET (Springel et al. 2001) to simulate mergers of isolated, low-redshift, gas-rich, identical disk galaxies, finding $C_{\rm rad} \simeq 1$. However, a higher value of $C_{\rm rad} = 2.75$ was found for disk-dominated galaxies that have recently experienced a major merger (Covington et al. 2011). In addition, Porter et al. (2014) used 68 hydrodynamical simulations of major and minor binary mergers (see Johansson et al. 2009) of galaxies with either mixed or spheroid-spheroid morphologies. They found that the morphology, the mass ratio and the gas content could cause the $C_{\rm rad}$ parameter to vary significantly, from 0.0 (dissipationless) for minor or major mergers where one or both of the progenitors are bulge-dominated; to 2.5 for major mergers between disk-dominated galaxies. In the current work we adopt the value $C_{\rm rad} = 0.1$ as it appears to best reproduce the mass-size relation of our galaxies, especially at the low-mass end (see Section 3.6.2).

2.3.2 Pseudo-bulges

Galaxy-galaxy interactions have a pivotal role in regulating galactic evolution, however internal processes, such as disk instabilities, are of similar importance since they are responsible for the emergence of pseudo-bulges out of disk material.

In order to determine the half-mass radius of the resulting pseudo-bulge we distinguish between two cases; the first is when the disk already possesses a bulge and then becomes unstable. We follow Guo et al. (2011) and assume that the unstable mass merges into the existing bulge, thus the final bulge's half-mass radius is given by:

$$G\frac{M_{\rm final}^2}{R_{\rm final}} = G\frac{M_{\rm old}^2}{R_{\rm old}} + G\frac{M_{\star,\rm unstable}^2}{R_{\rm b}} + 2\alpha_{\rm inter} \cdot G\frac{M_{\rm old} \cdot M_{\star,\rm unstable}}{R_{\rm old} + R_{\rm b}}\,, \tag{19}$$

where $M_{\rm final}$ and $R_{\rm final}$ are the mass and half-mass radius of the final bulge, $M_{\rm old}$ and $R_{\rm old}$ are the mass and half-mass radius of the existing bulge, $M_{\star,\rm unstable}$ is the mass occurred from Equation 6, $\alpha_{\rm inter} = 2$ since there is no relative motion between the old bulge and the unstable material and the half-mass radius of the unstable material $R_{\rm b}$ is taken from:

$$M_{\star,\rm unstable} = 2\pi \cdot \Sigma_{\star,0} \cdot R_{\rm d,\star} \cdot \left[R_{\rm d,\star} - (R_{\rm b} + R_{\rm d,\star}) \cdot \exp(-R_{\rm b}/R_{\rm d,\star})\right], \tag{20}$$

where $\Sigma_{\star,0}$ and $R_{\rm d,\star}$ are the central surface density and the exponential scale length of the disk. If the galaxy had no bulge prior to the instability incident we assume that the half-mass radius of the newly formed bulge is equal to $R_{\rm b}$.

3 RESULTS

3.1 Stellar mass assembly channels

One feature of our model is its ability to follow the formation and evolution of classical and pseudo-bulges by separately tracking each channel that contributes to their mass budget. This allows us to gain insight into the behaviour of each component and answer questions such as: how often disk galaxies host classical as opposed to pseudo-bulges; how is the mass of early- and late-type galaxies distributed; and how structurally different are galaxies that host classical and pseudo-bulges.

We follow the stellar mass transferred between galaxies in minor and major mergers, and the stellar mass transferred between galactic components during disk instability events. We split the total stellar mass into 6 categories, some of which are subsets of others:

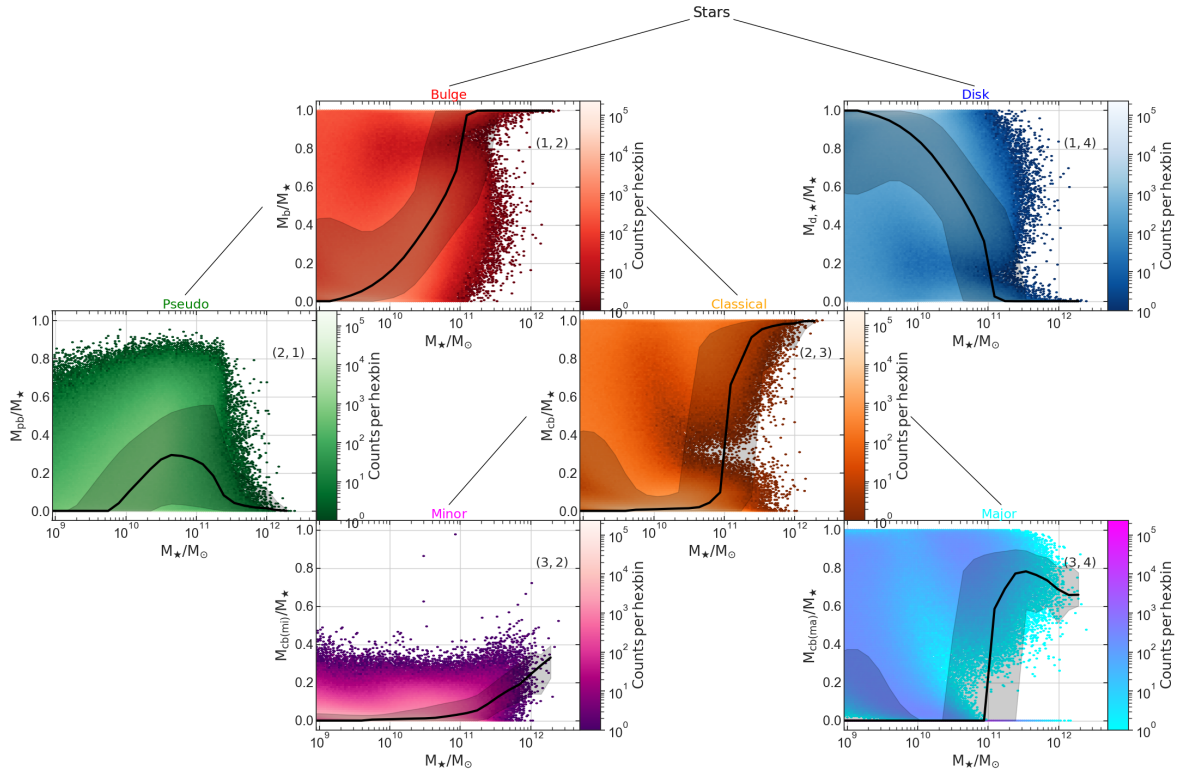

Figure 1. Decomposition of the total stellar mass of each galaxy at z ∼ 0.0. Each panel contains a hexagonal binning plot of the component-to-total stellar mass ratio as a function of the total stellar mass along with the median (black solid lines) and the $16^{\text{th}} - 84^{\text{th}}$ percentile range (black shaded regions). The black straight lines that connect the panels represent the divisions described in the tree chart in Section 3.1 and the (row, column) positioning of each component in the figure corresponds to: (1,2) – bulge; (1,4) – disk; (2,1) – pseudo-bulge; (2,3) – classical-bulge; (3,2) – through minor mergers; (3,4) – through minor mergers.

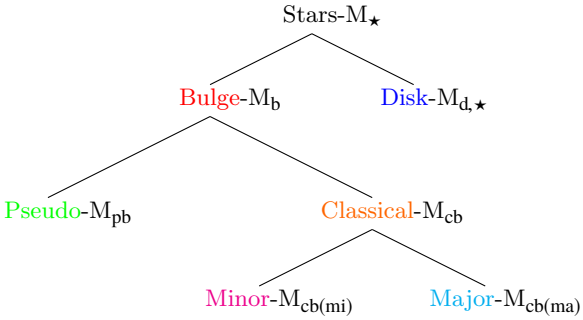

In the L-GALAXIES model stars can be found in the two main galactic components, namely the stellar disk (d) and the bulge (b). Tracking the two widely accepted bulge formation paths allows us to further divide the bulge mass into the mass created through disk instabilities and the one accreted through mergers, hence leading to the formation of pseudo-bulges (pb) and classical bulges (cb), respectively. Finally, the population of classical bulges can be dichotomised into those produced through major mergers (cb(ma)) and those through minor mergers (cb(mi)). This decomposition is shown in Fig. 1 which contains the ratio between the stellar mass of each of the above 6 components and the total stellar mass of each galaxy.

As can be seen in Fig. 1, the L-GALAXIES model produces pure disk- (1,4) with masses up to $M_\star \sim 3{\cdot}10^{11}\,\mathrm{M}_\odot$ and pure bulge-dominated galaxies (1,2) of all masses. The corresponding median lines suggest that the most massive galaxies are bulge-dominated (e.g., Baldry et al. 2004; Wilman & Erwin 2012; Nair & Abraham 2010), while the majority of normal galaxies are disk-dominated (e.g., Fukugita et al. 2007; Bamford et al. 2009; Nair & Abraham 2010); a behaviour which is consistent with observational studies. The large scatter in (2,1) suggests that in a few galaxies pseudo-bulges dominate the total stellar mass budget, hence leading to the development of lenticular galaxies (Kormendy & Kennicutt 2004; Kormendy & Cornell 2004; Weinzirl et al. 2009; Vaghmare et al. 2013). Interestingly, there are a some extreme cases where the pseudo-bulge-to-total stellar mass ratio is as high as 0.9. This is in agreement with the recent work of Saha & Cortesi (2018) who proposed disk instabilities as a mechanism responsible for the production of field S0 galaxies. From the behaviour of our data in panels (2,1) and (2,3) and the corresponding median lines, we can say that most of the bulge mass in galaxies with masses between $10^{10}\,\mathrm{M}_\odot < M_\star < 10^{11}\,\mathrm{M}_\odot$ is in pseudo- and not classical bulges. At $\sim 10^{11}\,\mathrm{M}_\odot$ the secular evolution scenario cannot compete with the violent one and as a consequence major mergers (3,4) begin to destroy the progenitors and form bulge-dominated systems (2,3). Finally, we note that minor mergers (3,2) increase in importance in the largest galaxies.

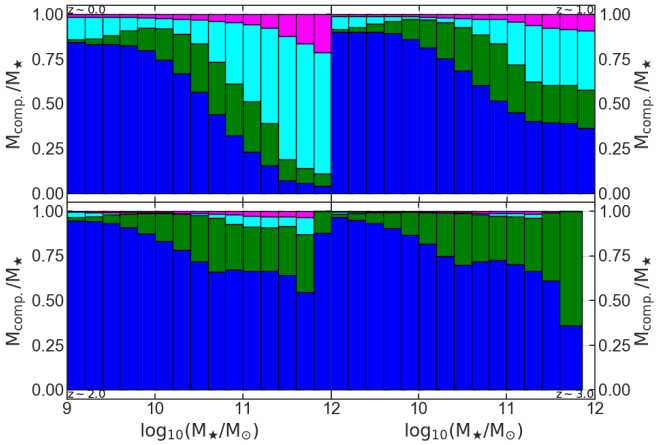

Figure 2. Relative contribution of each component to the total stellar mass at redshifts $z \sim 0.0$, 1.0, 2.0 and 3.0. Colors are the same as in Fig. 1: blue – disk; green – pseudo-bulge; cyan – classical bulge through major mergers; magenta – classical bulge through minor mergers.

3.2 Evolution of stellar mass assembly channels

Fig. 2 illustrates how the contribution of each component to the total stellar mass fluctuates within each galactic mass range at different redshifts.

At $z \sim 0.0$ at the lowest masses about 80 percent of stars lie in disks with most of the rest in merger-driven bulges. At $10^{10}\,\mathrm{M}_\odot$ minor mergers begin to ignite the formation of classical bulges and for total stellar masses above $10^{11}\,\mathrm{M}_\odot$ major mergers become the dominant mechanism that affect galactic morphology. This behaviour follows from a hierarchical galaxy assembly scenario in which mergers give rise to the formation of the most massive system. Pseudo-bulges never dominate but are most important between $10^{10}\,\mathrm{M}_\odot$ and $10^{11.5}\,\mathrm{M}_\odot$, accounting for about 30 percent of the total over this range. In this mass range we can also see a mixture of pseudo- and classical bulges. Indeed, as discovered by a few studies (e.g., Nowak et al. 2010; Méndez-Abreu et al. 2014; Erwin et al. 2015), the two-path picture of bulge formation does not exclude the fact that there are galaxies which host composite bulges (i.e., coexisting classical and pseudo-bulges).

As pointed out by few authors (e.g., Bell et al. 2004; Conselice et al. 2005; Ilbert et al. 2010) the massive end of the galaxy mass function at $z < 0.8$ is dominated by galaxies with early-type morphologies, which is consistent with our results. Furthermore, studies which focused on the evolution of the merger rate of galaxies (e.g., Le Fèvre et al. 2000; Bell et al. 2006; Lotz et al. 2008) concluded that the majority of them have experienced major mergers since $z \sim 1$, and this event has severely affected their morphology (van Dokkum 2005). In galaxies produced by the L-Galaxies model we can also notice that classical bulges, both via major and minor merger, have a significant contribution to the total stellar mass at $z \leq 1$, while the disk component becomes increasingly important at higher redshifts.

3.3 Galactic morphology

In the L-Galaxies SAM mergers are dichotomised into major and minor, where the morphology of the resulting galaxy will be strongly related to the mass ratio of the merging galaxies. If the total baryonic mass (stars+gas) of the more massive progenitor exceeds that of the less massive by at least an order of magnitude, then this incident is characterised as minor; in any other case the merger is treated as a major. In this work we adopt the same mass ratio threshold ($R_{\mathrm{merger}} \equiv M_{\mathrm{sat.}}/M_{\mathrm{cen.}} = 0.1$) as in HWT15 in order to distinguish those two regimes. The most apparent consequence of this division is that it regulates the type of the remnant galaxy (i.e., bulge- or disk-dominated).

3.3.1 Types of galaxies

This categorisation is depicted in the left panel of Fig. 3 which represents the fraction of different galaxy types as a function of their total stellar mass. We split our galaxy sample into three categories based on their bulge-to-total stellar mass ratio. Red solid line shows the fraction of bulge-dominated galaxies, akin to ellipticals ($M_{\mathrm{b}}/M_\star > 0.7$), blue solid line shows the fraction of normal spirals ($0.01 < M_{\mathrm{b}}/M_\star < 0.7$) and green solid line represents disk-dominated galaxies, akin to pure disks or extreme late-types ($M_{\mathrm{b}}/M_\star < 0.01$). Similar proxies for the morphology of simulated galaxies have been used by several authors and even though they seem arbitrary, in general the results do no depend significantly on them (e.g., Bertone et al. 2007; Lagos et al. 2008; Guo et al. 2011; Gargiulo et al. 2015).

The observational data have been taken from Conselice (2006), where he used a sample of ~ 22,000 galaxies at $z < 0.05$ to plot the morphological fraction as a function of stellar mass. In addition, Kelvin et al. (2014) analysed a sample of 2,711 local ($0.025 < z < 0.06$) galaxies taken from the Galaxy And Mass Assembly (GAMA) survey. They visually divided their sample into 5 categories, namely LBS, E, S0-Sa, Sab-Scd and Sd-Irr, however in order to make the comparison with our data more efficient we combined the LBS with E galaxies and the S0-Sa with Sab-Scd galaxies (see Table 1 of Kelvin et al. 2014). We also include the HWT15 data (dotted lines) for comparison with the previous version of the model.

Both surveys indicate that the fractional contribution for galaxies with stellar masses between $10^9\,\mathrm{M}_\odot < M_\star < 10^{11}\,\mathrm{M}_\odot$ is dominated by spirals, although by $M_\star \sim 10^{10.5}\,\mathrm{M}_\odot$ spirals and ellipticals represent about 50% each. At stellar masses higher than that almost all galaxies have turned into ellipticals. These behaviours are also fairly well represented by our galaxies over the whole stellar mass range.

In the right panel we present the fraction of our disk- ($B/T < 0.3$) and bulge-dominated ($B/T > 0.3$) galaxies and compare with the fraction found by Moffett et al. (2016) who selected 4,971 disk-(Sab-Scd/Sd-Irr) and 1,692 spheroid-dominated (E/S0-Sa) galaxies. The motivation for using the above selection criteria is provided by various studies who investigated the B/T ratio of S0 galaxies (e.g. Laurikainen et al. 2005, 2010; Barway et al. 2016) and found that the mean value is ~ 0.25. In addition, Weinzirl et al. (2009) found that, in their sample, the fraction of spiral galaxies with

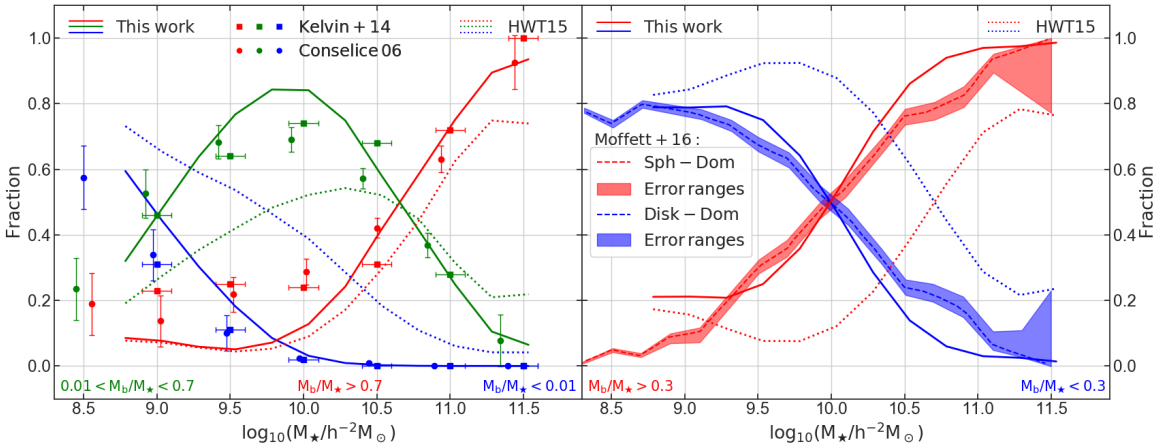

Figure 3. Fraction of different morphological types as a function of total stellar mass at z ∼ 0.0. Solid and dotted lines show results from this work and HWT15, respectively. **Left panel:** Red, green and blue lines show the fraction of bulge-dominated, normal spiral and pure disk galaxies, respectively. Red, green and blue filled circles are observational data from Conselice (2006) that show the elliptical, spiral and irregular galaxies, respectively. Red, green and blue squares are S0-Sa+Sab-Scd, LBS+E and Sd-Irr galaxies, respectively from Kelvin et al. (2014). **Right panel:** Red lines represent spheroid dominated galaxies, while blue lines represent disk dominated. Observational data points from Moffett et al. (2016) are represented by dashed lines along with the corresponding errors.

$0.2 < B/T < 0.75$ is 8%, while ∼ 65% of them have $B/T < 0.2$. Hence, these results and the fact that Moffett et al. (2016) included S0 galaxies in their spheroid-dominated sample reinforce our approach of using the aforementioned thresholds for our analysis.

Our results suggest that the point indicating the transition between the numerical dominance of disk- and spheroid-dominated galaxies is in strong agreement with Moffett et al. (2016) and shows a clear improvement over the HWT15 version of the L-Galaxies SA model.

3.3.2 Stellar mass function

The left panel in Fig. 4 presents the stellar mass fuction for our whole dataset, while in the right panel we split our galaxies into the three different morphological types. Similar plots have been made by Kelvin et al. (2014) (see their Figure 4) and Moffett et al. (2016) (see their Figure 8) and their results show similar behaviour. From this we see that the flattening of the mass function towards the knee at $10^{10}h^{-1}$ $M_\odot$ is associated with the transition from disk-dominated galaxies to those that have a significant pseudo-bulge component.

We note that taking into account angular momentum losses during cooling results in smaller gas disk radii (Equation 2) which lower the star formation threshold (Equation 4) and allow our galaxies to produce more stars (Equation 3). In addition, the new galactic instability scheme modifies the mass of gas and stars by redistributing them between galactic components. Therefore, the combination of those two processes directly affects the galactic morphology and allows us to better match the observed behaviours.

3.4 Mass-spin relation

Angular momentum is one of the most fundamental galactic properties; it can dictate the galactic size and morphology, and also provides a vital constraint on theories of galaxy formation (e.g., Mo et al. 1998; Romanowsky & Fall 2012; Obreschkow & Glazebrook 2014; Sweet et al. 2018; Posti et al. 2018). The correlation of the specific angular momentum with stellar mass, $j \propto M^{2/3}$, was introduced 35 years ago by Fall (1983).

We show this relation in Fig. 5 for our disk-dominated galaxies ($M_{\mathrm{d},\star}/M_\star > 0.7$). We also include results from Obreschkow & Glazebrook (2014) who analysed 16 nearby spiral galaxies of the The HI Nearby Galaxy Survey (THINGS) sample (Walter et al. 2008), and Fall & Romanowsky (2013) who focused on 64 galaxies from type Sa to Sm from the Kent (1986, 1987, 1988) datasets, and find that our simulated galaxies follow closely the Fall (1983) relation and are in very good agreement with the observations.

In Fig. 6 we calculate the total specific angular momentum of each galaxy as $j_\star = (j_{\mathrm{d},\star}M_{\mathrm{d},\star} + j_{\mathrm{b}}M_{\mathrm{b}})/(M_{\mathrm{d},\star} + M_{\mathrm{b}})$ and plot it as a function of the total stellar mass. The different colors represent the $M_{\mathrm{b}}/M_\star$ ratio of the corresponding galaxy. We compare our results with Fall & Romanowsky (2018) who presented their sample of 57 spirals, 14 lenticulars and 23 ellipticals. The behaviour of our data indicate that the more disk-dominated galaxies (i.e., lower $M_{\mathrm{b}}/M_\star$ values) rotate faster than the bulge-dominated, hence we find an impressive agreement with the observed trends.

3.5 Black hole-bulge mass relation

The fact that black holes and bulges (either classical or pseudo) are formed in associated processes results in tight relations between them (e.g., Magorrian et al. 1998; Kormendy & Gebhardt 2001; Beifiori et al. 2012, and references

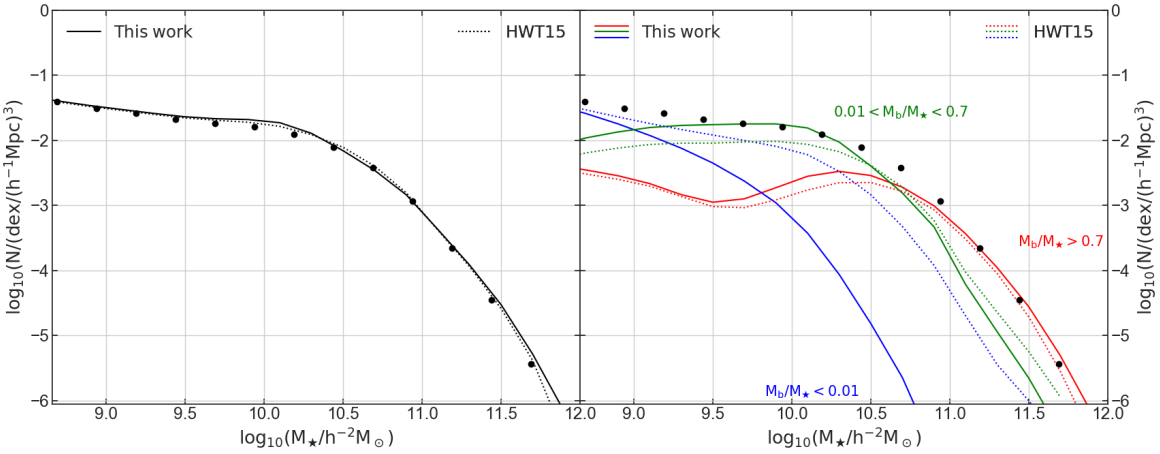

Figure 4. Stellar mass function at z ∼ 0.0. **Left panel:** Black solid line shows the stellar mass function for the whole L-Galaxies dataset. **Right panel:** Red, green and blue solid lines represent the stellar mass functions split into bulge-dominated, normal spiral and disk dominated galaxies. In both panels solid lines show predictions from our new model and dotted lines from HWT15; the black circles represent the combined observational data used to constrain the MCMC in HWT15.

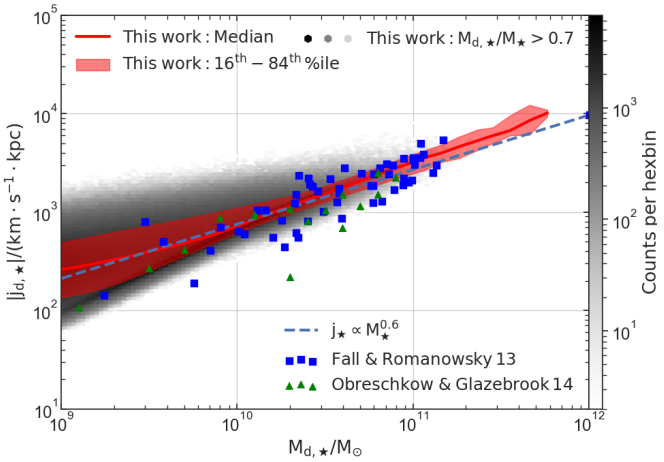

Figure 5. Stellar mass versus specific angular momentum for disk-dominated galaxies at redshift z ∼ 0.0, compared with Obreschkow & Glazebrook (2014) and Fall & Romanowsky (2013) observations and the Fall (1983) relation.

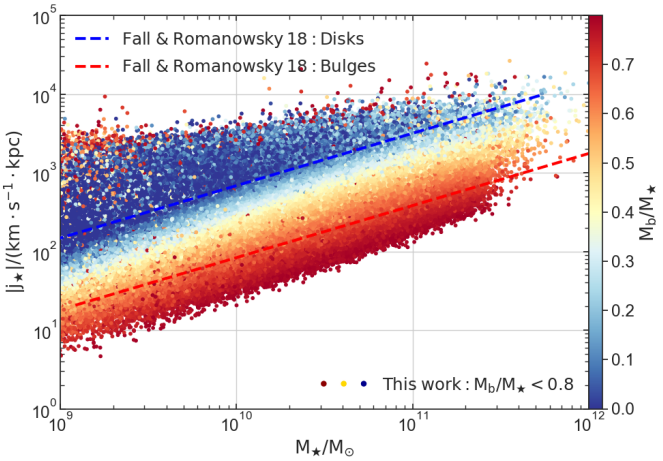

Figure 6. Stellar mass versus total specific angular momentum for $M_b/M_\star < 0.8$ galaxies at redshift z ∼ 0.0, compared with Fall & Romanowsky (2018) fit lines for disks and bulges. The colour of the symbols indicate different $M_b/M_\star$ values.

therein). Therefore, in this section we investigate the well known black hole-bulge mass relation (e.g., Marconi & Hunt 2003; Häring & Rix 2004) which is shown in Fig. 7.

We compare our simulated data with a sample of 30 nearby galaxies introduced by Häring & Rix (2004), 72 galaxies compiled by McConnell & Ma (2013) and 37 galaxies selected by Bentz & Manne-Nicholas (2018) from the Hubble Space Telescope images and deep, ground-based near-infrared images. Even though for $10^9\,M_\odot < M_b < 10^{10.5}\,M_\odot$ the L-Galaxies model predicts a large scatter in black hole masses, the majority of our galaxies form at all masses an almost linear relation in log-space (i.e., a power-law in linear-space) between black hole and bulge mass, as expected (e.g., Beifiori et al. 2012; Graham 2012; McConnell & Ma 2013). The magnitude of the scatter appears to decrease at higher masses, a behaviour which has been mentioned in previous studies and linked to mergers (e.g., Peng 2007; Hirschmann et al. 2010; Jahnke & Macciò 2011).

In this work we updated the processes responsible for the growth of bulges via mergers and disk instabilities; where the latter mechanism feeds a percentage of the unstable cold gas into the central super-massive black hole. Hence, Fig. 7 provides a sanity check for our new model since it dictates that the L-Galaxies model is still able to reproduce the tight black hole-bulge mass relation and shows an impressive agreement with the observational data at all masses.

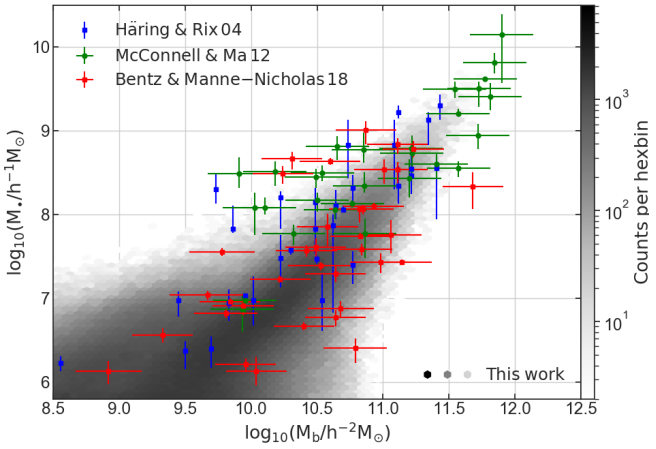

Figure 7. Black hole-bulge mass relation at z ~ 0.0. Black hexagons represent our galaxies; blue, green and red circles are observations from Häring & Rix (2004), McConnell & Ma (2013) and Bentz & Manne-Nicholas (2018), respectively.

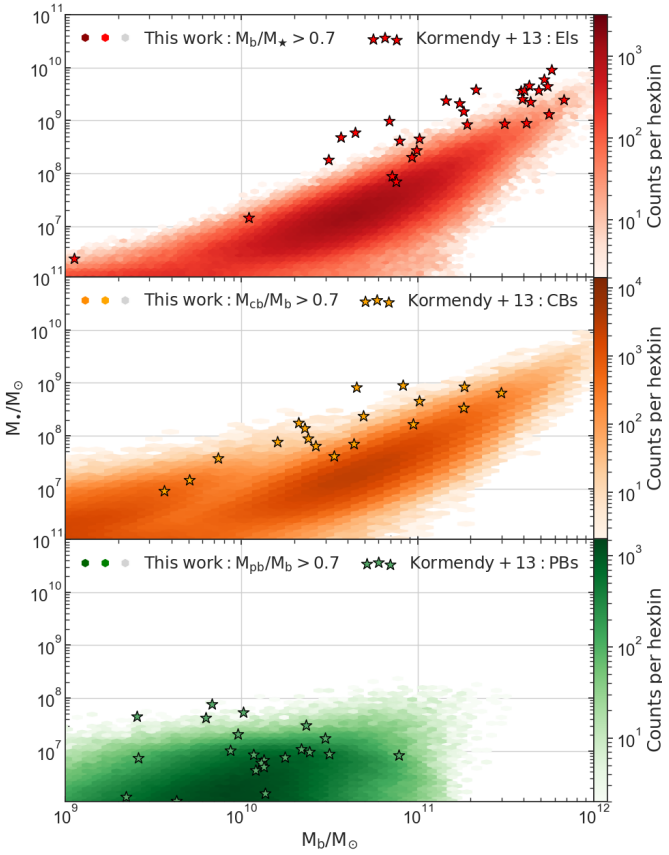

Figure 8. Black hole-bulge mass relation at z ~ 0.0 for bulge-dominated (top panel), classical bulge-dominated (middle panel) and pseudo-bulge-dominated (bottom panel) galaxies. Stars are observational data from Kormendy & Ho (2013).

3.5.1 A more detailed black hole-bulge mass relation

Several authors (e.g., Gadotti & Kauffmann 2009; Greene et al. 2008; Hu 2009; Sani et al. 2011; Shankar et al. 2012) studied the scaling relations between the supermassive black holes mass and the bulge mass in elliptical galaxies, classical bulges, and pseudo-bulges. The top and bottom panels of Fig. 8 represent the black hole-bulge mass relation for bulge-dominated galaxies (i.e., $M_{\rm b}/M_{\star} > 0.7$) and pseudo-bulge-dominated bulges (i.e., $M_{\rm pb}/M_{\rm b} > 0.7$), respectively. For the middle panel we combined the bulge mass produced by minor and major merger into a single component (i.e., $M_{\rm cb} = M_{\rm cb(ma)} + M_{\rm cb(mi)}$) and trim our galaxies by using a $M_{\rm cb}/M_{\rm b} > 0.7$ criterion.

The black hole-bulge mass relation displayed in each panel of Fig. 8 is in good agreement with the trends denoted by data from Kormendy & Ho (2013) which represent 87 galaxies observed by the Hubble Space Telescope. However, the normalisation is about 5 times lower than the observations, in apparent contradiction with the good agreement seen in Fig. 7.

Shankar et al. (2016) argued that the normalisation of the $M_{\bullet} - M_{\rm b}$ relation can be higher than the intrinsic one as a consequence of selection effects, and proposed that their Monte Carlo results constrain the normalisation to be a factor of ~50 to 100 lower when expressing black hole masses as a function of stellar or bulge mass (see also Bernardi et al. 2007, for a discussion about selection biases). In the L-Galaxies model one may adjust the free parameters which affect the efficiency of the black hole growth to better match the observation; in this work we decided not to modify them and keep the values that resulted from the HWT15 MCMC analysis.

3.6 Mass-size relation

3.6.1 Late-type galaxies

In Fig. 9 we present the stellar half-mass radius as a function of the total stellar mass for late-type galaxies. In this work we define late-type galaxies as those that have $M_{\rm d,\star}/M_{\star} > 0.7$; in other words the disk-dominated galaxies. We compare our galaxies with the following works:

- Shen et al. (2003): selected galaxies with $c < 2.86$ from 140,000 SDSS DR1 (York et al. 2000) galaxies at $z < 0.3$.
- Zhang & Yang (2017): selected 424,363 galaxies with $c < 2.85$ from the New York University Value-Added Galaxy Catalog at $z < 0.2$ (Blanton et al. 2005).
- Kalinova et al. (2017): selected slow-rising class galaxies (akin to late-type) based on the shapes and amplitude of the circular velocity curve of 238 CALIFA galaxies at $z < 0.03$ (Falcón-Barroso et al. 2017).

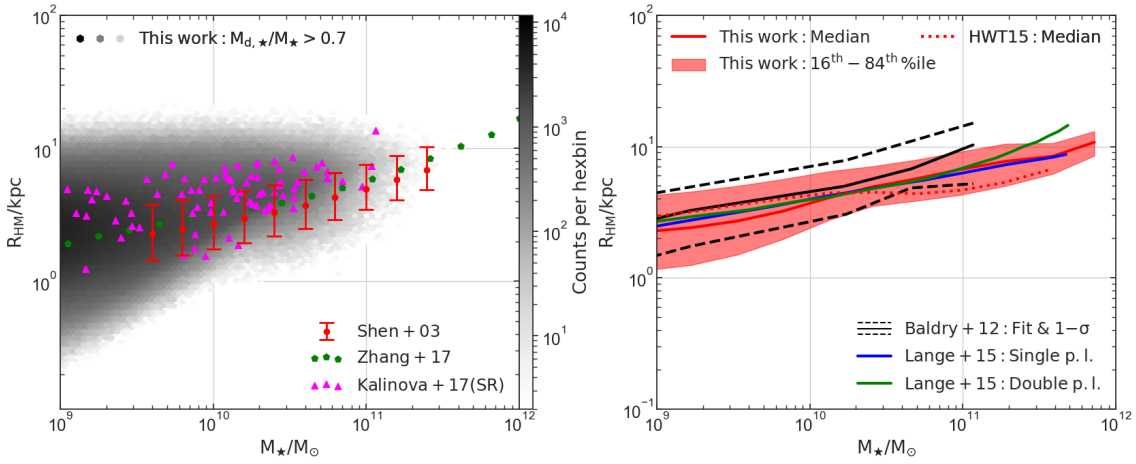

Figure 9. Mass-size relation for disk-dominated galaxies at $z \sim 0.1$. **Left panel:** Total stellar mass versus stellar half-mass radius compared with Shen et al. (2003); Zhang & Yang (2017) and Kalinova et al. (2017). **Right panel:** The median and $16^{th} - 84^{th}$ percentile range of the aforementioned relation compared with Baldry et al. (2012) and Lange et al. (2015) fit lines. Red solid and dotted lines show results from this work and HWT15, respectively.

- Baldry et al. (2012): selected late-type galaxies based on colour-magnitude diagrams of 5,210 GAMA galaxies at $z < 0.06$ (Driver et al. 2011).
- Lange et al. (2015): selected late-type galaxies by visually classifying GAMA II galaxies in the redshift range $0.01 < z < 0.1$ (Liske et al. 2015).

As explained in Section 2.1, we assume that the cold gas loses a fraction of its specific angular momentum to the dark matter halo during the cooling process, hence the cold gas disks are expected to be more compact than those produced by HWT15: this trait is then inherited by the stellar disks. In addition, instabilities in the gas disks can lead to star formation in the galactic disks and alter both their stellar mass and half-mass radius. For those reasons, the results show a significant improvement over past modelling attempts (e.g., top panel of Figure 2 and left panel of Figure 4 of Guo et al. 2011; Tonini et al. 2016, respectively), giving smaller disk half mass radii, especially at the low mass end where gas-rich galaxies are more frequent.

3.6.2 Early-type galaxies

The HWT15 model gives early-type galaxy sizes that are too large for a given mass. That motivated us to introduce energy dissipation in gas rich mergers, as described in Section 2.3.1. The result of that is shown in Fig. 10 where we show the total stellar mass versus stellar half-mass radius for galaxies with $M_{\rm cb(ma)}/M_\star > 0.7$. This sample contains galaxies which composed most of their stellar mass through major mergers, akin to ellipticals. We compare with the following observational data sets:

- Shen et al. (2003): selected galaxies with $c > 2.86$ from 140,000 SDSS DR1 (York et al. 2000) galaxies at $z < 0.3$.
- Chen et al. (2010): selected about 100 early-type galaxies that populate the red sequence in the Virgo cluster from SDSS DR5 (Adelman-McCarthy et al. 2007).
- Zhang & Yang (2017): selected 424,363 galaxies with $c > 2.85$ from the New York University Value-Added Galaxy Catalog at $z < 0.2$ (Blanton et al. 2005).
- Forbes et al. (2017): selected galaxies from the SLUGGS survey which targeted 25 nearby ($D \leq 25$ Mpc) massive early-type galaxies in different environments (Brodie et al. 2014).
- Cappellari et al. (2013): selected 260 early-type galaxies from the ATLAS^{3D} project at $z = 0$ (Cappellari et al. 2011).
- Gadotti (2009): selected galaxies with $c > 2.5$ from the SDSS DR2 (Abazajian et al. 2004).
- Lange et al. (2015): selected early-type galaxies by visually classifying GAMA II galaxies in the redshift range $0.01 < z < 0.1$ (Liske et al. 2015).

The updated merger remnant size recipe introduced in this work gives more compact remnant sizes at the low-mass end compared to HWT15 which over-predicted the size of the smallest galaxies. We can clearly see that our median line agrees well with a single power law for masses below $10^{10}\,M_\odot$, as indicated by Lange et al. (2015). However, at the high mass end we do not see the sharp upturn in size indicated by their double power-law model. We note that there is an increase in intracluster light in the most massive halos that we do not include in our analysis.

3.6.3 The dependence of disk scale length on morphology

In Fig. 11 we present three different versions of the disk scale length versus mass relation. The left panel contains our median lines for 4 different bulge-to-total stellar mass ratios and Gadotti (2009) galaxies color-coded by their B/T luminosity ratio. The L-Galaxies model shows adequate agreement with the observed behaviour at all masses, which indicates that the disk scale lengths decrease as the B/T ratio increases.

For the right panel we selected galaxies in which the classical or the pseudo-bulge is the dominant bulge component, i.e., $M_{\rm cb}/M_{\rm b} > 0.7$ or $M_{\rm pb}/M_{\rm b} > 0.7$, respectively.

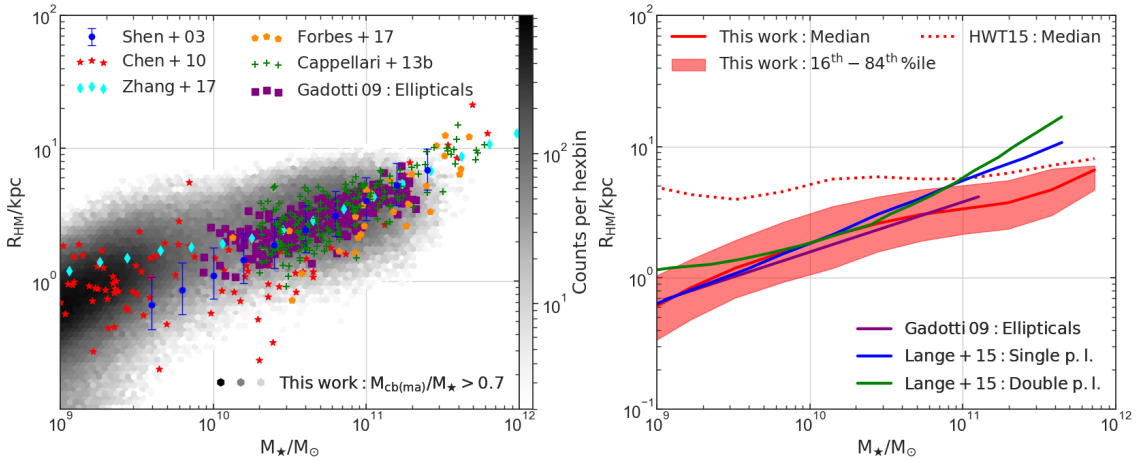

Figure 10. Mass-size relation for early-type galaxies at $z \sim 0.1$. **Left panel:** Total stellar mass versus stellar half-mass radius for early-type galaxies compared with Shen et al. (2003); Chen et al. (2010); Zhang & Yang (2017); Forbes et al. (2017); Cappellari et al. (2013) and Gadotti (2009). **Right panel:** The median and $16^{th} - 84^{th}$ percentile range of the aforementioned relation compared with fitting lines from Gadotti (2009) and Lange et al. (2015). Red solid and dotted lines show results from this work and HWT15, respectively.

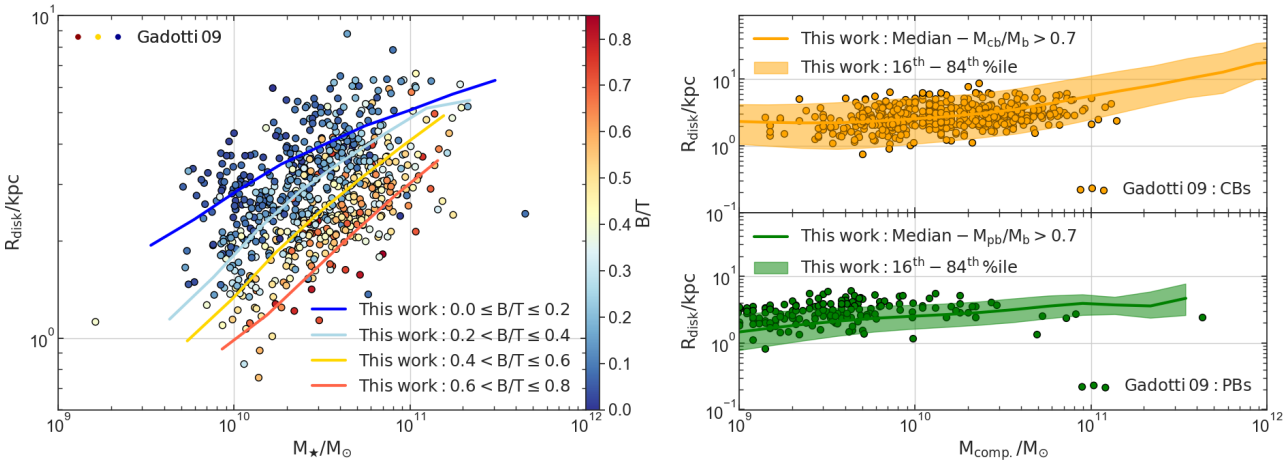

Figure 11. Disk scale length as a function of mass at $z \sim 0.05$. **Left panel:** Total stellar mass versus disk scale length compared with Gadotti (2009) galaxies colored by different B/T ratios. **Right panel:** Classical and pseudo-bulge mass against disk scale length compared with Gadotti (2009) classical and pseudo-bulges, respectively.

Gadotti (2009) fitted different profiles in each galaxy image in his sample. He used a bulge profile which is described by a Sersic (1968) function; when n = 4 the profile is a de Vaucouleurs (1948), while n = 1 corresponds to an exponential bulge (i.e., pseudo-bulge). We find a strong agreement with the observed trends which suggests that, as expected, galaxies with more extended disks tend to be more massive. This slope appears to be steeper for galaxies that host classical instead of pseudo-bulges, however, we notice that, in the L-Galaxies model, galaxies that host the latter appear to have slightly smaller disk scale lengths than is observed.

3.7 The Tully-Fisher relation

The Tully-Fisher relation (Tully & Fisher 1977) describes an empirical correlation between the intrinsic luminosity and the emission line width of rotating spiral galaxies. A more useful form for our purposes has been proposed by McGaugh et al. (2000) that relates the total baryonic mass and the rotation velocity.

In this work we adopt, for simplicity, as the typical rotation velocity for both the gaseous and the stellar disk, the maximum circular velocity of the surrounding dark matter halo (V_c). This assumption is in agreement with Tissera et al. (2010) who found that the maximum circular velocities of dark matter haloes is very similar to the maximum rota-

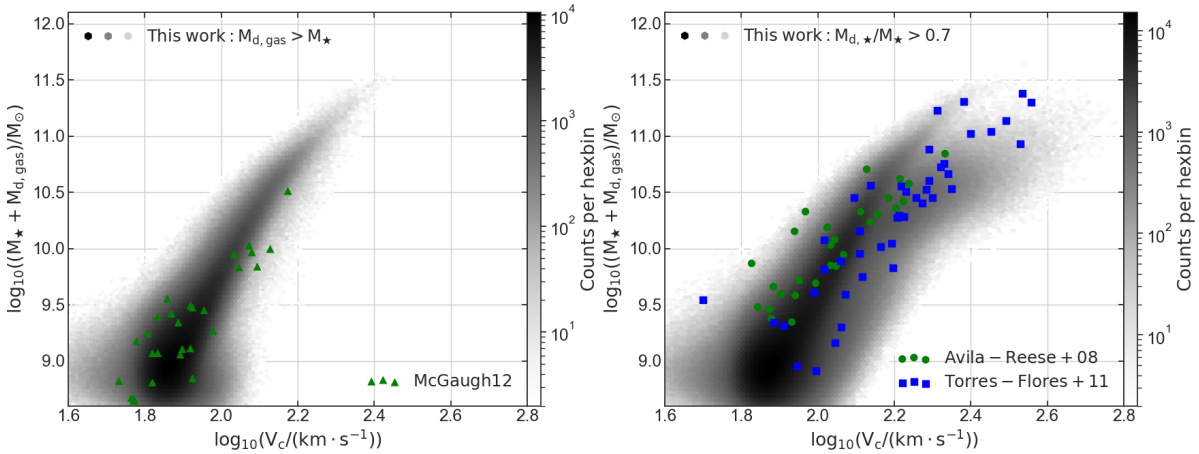

Figure 12. Baryonic Tully-Fisher relation at $z \sim 0.0$. **Left panel:** Gas-dominated galaxies compared with a dataset from McGaugh (2012). **Right panel:** Disk-dominated galaxies compared with Avila-Reese et al. (2008) and Torres-Flores et al. (2011).

tion velocities of disks. In the left panel of Fig. 12 we compare gas-dominated (i.e., $M_{\rm d,gas} > M_\star$) galaxies produced by the L-Galaxies model with the dataset used by McGaugh (2012) which consist of gas dominated galaxies from Begum et al. (2008); Stark et al. (2009) and Trachternach et al. (2009). Furthermore, in the right panel we investigate the baryonic Tully-Fisher relation of disk-dominated galaxies (i.e., $M_{\rm d,\star}/M_\star > 0.7$) where we include observations from Avila-Reese et al. (2008) (normal, non–interacting disk galaxies compiled from the literature and homogenized in Zavala et al. 2003) and Torres-Flores et al. (2011) (spiral and irregular galaxies from Gassendi HAlpha survey of SPirals, GHASP Epinat et al. 2008b,a).

As shown in both panels of Fig. 12, our galaxies follow a tight relation that is in close agreement with the observational data. However, in the right panel we notice that some of the galaxies with the highest circular velocities appear to be less massive than those observed by Avila-Reese et al. (2008) and Torres-Flores et al. (2011). This results from the fact that for baryonic masses $\log_{10}((M_\star + M_{\rm d,gas})/{\rm M}_\odot) > 10$ our galaxies split into two groups, where the lower one represents extremely gas poor quiescent galaxies whose contribution to the total baryonic mass is not significant.

4 CONCLUSIONS

This paper addresses some deficiencies in the otherwise very successful Henriques et al. (2015) SA model with regard to bulge formation via disk instabilities and merger remnant sizes. In making the latter change, we drew inspiration from the work of Covington et al. (2008, 2011) and Tonini et al. (2016). The main changes are:

- the specific angular momentum of accreted gas is reduced to 0.8 times that of the dark matter halo;
- an improved disk instability recipe that considers both the gas and the stars, rather than just the latter;
- the introduction of dissipation in gas-rich mergers.

Our main conclusions are as follows:

- The updated disk instability recipe allows us to have an impressive agreement with the observed fraction of different galactic morphologies.
- The stellar half-mass radius and spin of disk-dominated galaxies is in great agreement with the observed relations due to the reduction of the initial angular momentum of the gas disk.
- Highly dissipative mergers result in more compact remnants which match the observed mass-size relation of bulge-dominated galaxies.
- The tight relation between the stellar disk scale length and mass is still present after the assumption that the gas loses 20% of its initial specific angular momentum during cooling.
- The baryonic Tully-Fisher relation follows the observed single power law.

ACKNOWLEDGEMENTS

The authors contributed in the following way to this paper. DI undertook the vast majority of the coding and data analysis, and produced the figures. PAT supervised DI and together they drafted the paper. BMH and MTS provided input on content and helped with interpretation of the results. All authors helped to proof-read the text.

DI (ORCID 0000-0003-2946-8080) would like to acknowledge his family members for their continuous encouragement and financial support. PAT (ORCID 0000-0001-6888-6483) acknowledges support from the Science and Technology Facilities Council (grant number ST/P000525/1). The work of BMH (ORCID 0000-0002-1392-489X) was supported by Advanced Grant 246797 "GALFORMOD" from the European Research Council and by a Zwicky Fellowship. MTS acknowledges support from a Royal Society Leverhulme Trust Senior Research Fellowship (LT150041)

REFERENCES

Abazajian K., et al., 2004, AJ, 128, 502
Adelman-McCarthy J. K., et al., 2007, ApJS, 172, 634
Aguerri J. A. L., Balcells M., Peletier R. F., 2001, A&A, 367, 428
Andredakis Y. C., Sanders R. H., 1994, MNRAS, 267, 283
Andredakis Y. C., Peletier R. F., Balcells M., 1995, MNRAS, 275, 874
Athanassoula E., 2005, MNRAS, 358, 1477
Avila-Reese V., Zavala J., Firmani C., Hernández-Toledo H. M., 2008, AJ, 136, 1340
Baldry I. K., Glazebrook K., Brinkmann J., Ivezić Ž., Lupton R. H., Nichol R. C., Szalay A. S., 2004, ApJ, 600, 681
Baldry I. K., et al., 2012, MNRAS, 421, 621
Bamford S. P., et al., 2009, MNRAS, 393, 1324
Barnes J., Efstathiou G., 1987, ApJ, 319, 575
Barnes J. E., Hernquist L., 1996, ApJ, 471, 115
Barway S., Saha K., Vaghmare K., Kembhavi A. K., 2016, MNRAS, 463, L41
Baugh C. M., Cole S., Frenk C. S., 1996, MNRAS, 283, 1361
Begum A., Chengalur J. N., Karachentsev I. D., Sharina M. E., 2008, MNRAS, 386, 138
Beifiori A., Courteau S., Corsini E. M., Zhu Y., 2012, MNRAS, 419, 2497
Bell E. F., et al., 2004, ApJ, 608, 752
Bell E. F., Phleps S., Somerville R. S., Wolf C., Borch A., Meisenheimer K., 2006, ApJ, 652, 270
Benson A. J., 2012, New Astron., 17, 175
Bentz M. C., Manne-Nicholas E., 2018, preprint, (arXiv:1808.01329)
Bernardi M., Sheth R. K., Tundo E., Hyde J. B., 2007, ApJ, 660, 267
Bertin G., Romeo A. B., 1988, A&A, 195, 105
Bertone S., De Lucia G., Thomas P. A., 2007, MNRAS, 379, 1143
Bett P., Eke V., Frenk C. S., Jenkins A., Okamoto T., 2010, MNRAS, 404, 1137
Binney J., Tremaine S., 1987, Galactic dynamics
Blanton M. R., et al., 2005, AJ, 129, 2562
Blumenthal G. R., Faber S. M., Primack J. R., Rees M. J., 1984, Nature, 311, 517
Blumenthal G. R., Faber S. M., Flores R., Primack J. R., 1986, ApJ, 301, 27
Bournaud F., Jog C. J., Combes F., 2007, A&A, 476, 1179
Boylan-Kolchin M., Springel V., White S. D. M., Jenkins A., Lemson G., 2009, MNRAS, 398, 1150
Brodie J. P., et al., 2014, ApJ, 796, 52
Bryan G. L., et al., 2014, ApJS, 211, 19
Cacciato M., Dekel A., Genel S., 2012, MNRAS, 421, 818
Cappellari M., et al., 2011, MNRAS, 413, 813
Cappellari M., et al., 2013, MNRAS, 432, 1862
Carollo C. M., 1999, ApJ, 523, 566
Chen C.-W., Côté P., West A. A., Peng E. W., Ferrarese L., 2010, ApJS, 191, 1
Christodoulou D. M., Shlosman I., Tohline J. E., 1995, ApJ, 443, 551
Cole S., Aragon-Salamanca A., Frenk C. S., Navarro J. F., Zepf S. E., 1994, MNRAS, 271, 781
Cole S., Lacey C. G., Baugh C. M., Frenk C. S., 2000, MNRAS, 319, 168
Combes F., Sanders R. H., 1981, A&A, 96, 164
Combes F., Debbasch F., Friedli D., Pfenniger D., 1990, A&A, 233, 82
Conselice C. J., 2006, MNRAS, 373, 1389
Conselice C. J., Blackburne J. A., Papovich C., 2005, ApJ, 620, 564
Courteau S., de Jong R. S., Broeils A. H., 1996, ApJ, 457, L73
Covington M., Dekel A., Cox T. J., Jonsson P., Primack J. R., 2008, MNRAS, 384, 94
Covington M. D., Primack J. R., Porter L. A., Croton D. J., Somerville R. S., Dekel A., 2011, MNRAS, 415, 3135
Croton D. J., et al., 2006, MNRAS, 365, 11
Croton D. J., et al., 2016, ApJS, 222, 22
Dalcanton J. J., Spergel D. N., Summers F. J., 1997, ApJ, 482, 659
Danovich M., Dekel A., Hahn O., Ceverino D., Primack J., 2015, MNRAS, 449, 2087
De Lucia G., Blaizot J., 2007, MNRAS, 375, 2
Dekel A., Cox T. J., 2006, MNRAS, 370, 1445
Dekel A., et al., 2009, Nature, 457, 451
Djorgovski S., Davis M., 1987, ApJ, 313, 59
Driver S. P., et al., 2011, MNRAS, 413, 971
Dutton A. A., van den Bosch F. C., 2009, MNRAS, 396, 141
Efstathiou G., Lake G., Negroponte J., 1982, MNRAS, 199, 1069
Eliche-Moral M. C., Balcells M., Aguerri J. A. L., González-García A. C., 2006, A&A, 457, 91
Eliche-Moral M. C., González-García A. C., Balcells M., Aguerri J. A. L., Gallego J., Zamorano J., Prieto M., 2011, A&A, 533, A104
Elmegreen B. G., 1995, MNRAS, 275, 944
Elmegreen B. G., 2011, ApJ, 737, 10
Englmaier P., Shlosman I., 2004, ApJ, 617, L115
Epinat B., et al., 2008a, MNRAS, 388, 500
Epinat B., Amram P., Marcelin M., 2008b, MNRAS, 390, 466
Erwin P., et al., 2015, MNRAS, 446, 4039
Faber S. M., Jackson R. E., 1976, ApJ, 204, 668
Fabricius M. H., Saglia R. P., Fisher D. B., Drory N., Bender R., Hopp U., 2012, ApJ, 754, 67
Falcón-Barroso J., et al., 2017, A&A, 597, A48
Fall S. M., 1983, in Athanassoula E., ed., IAU Symposium Vol. 100, Internal Kinematics and Dynamics of Galaxies. pp 391–398
Fall S. M., 2002, in Da Costa G. S., Sadler E. M., Jerjen H., eds, Astronomical Society of the Pacific Conference Series Vol. 273, The Dynamics, Structure and History of Galaxies: A Workshop in Honour of Professor Ken Freeman. p. 289 (arXiv:astro-ph/0203492)
Fall S. M., Efstathiou G., 1980, MNRAS, 193, 189
Fall S. M., Romanowsky A. J., 2013, ApJ, 769, L26
Fall S. M., Romanowsky A. J., 2018, preprint, (arXiv:1808.02525)
Fisher D. B., 2006, ApJ, 642, L17
Fisher D. B., Drory N., 2008, AJ, 136, 773
Fisher D. B., Drory N., 2016, in Laurikainen E., Peletier R., Gadotti D., eds, Astrophysics and Space Science Library Vol. 418, Galactic Bulges. p. 41 (arXiv:1512.02230), doi:10.1007/978-3-319-19378-6_3
Fisher D. B., Drory N., Fabricius M. H., 2009, ApJ, 697, 630
Flores R., Primack J. R., Blumenthal G. R., Faber S. M., 1993, ApJ, 412, 443
Forbes D. A., Sinpetru L., Savorgnan G., Romanowsky A. J., Usher C., Brodie J., 2017, MNRAS, 464, 4611
Friedli D., Benz W., 1995, A&A, 301, 649
Fukugita M., et al., 2007, AJ, 134, 579
Gadotti D. A., 2009, MNRAS, 393, 1531
Gadotti D. A., Kauffmann G., 2009, MNRAS, 399, 621
Gargiulo I. D., et al., 2015, MNRAS, 446, 3820
Ghosh S., Jog C. J., 2015, MNRAS, 451, 1350
Goldbaum N. J., Krumholz M. R., Forbes J. C., 2016, ApJ, 827, 28
Gonzalez-Perez V., Lacey C. G., Baugh C. M., Lagos C. D. P., Helly J., Campbell D. J. R., Mitchell P. D., 2014, MNRAS, 439, 264
Governato F., et al., 2009, MNRAS, 398, 312
Goz D., Monaco P., Murante G., Curir A., 2014, preprint, (arXiv:1412.2883)
Graham A. W., 2012, ApJ, 746, 113

Greene J. E., Ho L. C., Barth A. J., 2008, ApJ, 688, 159
Guedes J., Mayer L., Carollo M., Madau P., 2013, ApJ, 772, 36
Guo Q., et al., 2011, MNRAS, 413, 101
Häring N., Rix H.-W., 2004, ApJ, 604, L89
Hatton S., Devriendt J. E. G., Ninin S., Bouchet F. R., Guiderdoni B., Vibert D., 2003, MNRAS, 343, 75
Hawarden T. G., Mountain C. M., Leggett S. K., Puxley P. J., 1986, MNRAS, 221, 41P
Henriques B. M. B., White S. D. M., Thomas P. A., Angulo R. E., Guo Q., Lemson G., Springel V., 2013, MNRAS, 431, 3373
Henriques B. M. B., White S. D. M., Thomas P. A., Angulo R., Guo Q., Lemson G., Springel V., Overzier R., 2015, MNRAS, 451, 2663
Hernquist L., Katz N., 1989, ApJS, 70, 419
Hirschmann M., Khochfar S., Burkert A., Naab T., Genel S., Somerville R. S., 2010, MNRAS, 407, 1016
Ho L. C., 2008, ARA&A, 46, 475
Hoffmann V., Romeo A. B., 2012, MNRAS, 425, 1511
Holmes L., et al., 2015, MNRAS, 451, 4397
Hopkins P. F., Cox T. J., Younger J. D., Hernquist L., 2009a, ApJ, 691, 1168
Hopkins P. F., Hernquist L., Cox T. J., Keres D., Wuyts S., 2009b, ApJ, 691, 1424
Hopkins P. F., Bundy K., Hernquist L., Wuyts S., Cox T. J., 2010a, MNRAS, 401, 1099
Hopkins P. F., et al., 2010b, ApJ, 715, 202
Hu J., 2009, preprint, (arXiv:0908.2028)
Ilbert O., et al., 2010, ApJ, 709, 644
Jahnke K., Macciò A. V., 2011, ApJ, 734, 92
Jog C. J., 1996, MNRAS, 278, 209
Jog C. J., Solomon P. M., 1984a, ApJ, 276, 114
Jog C. J., Solomon P. M., 1984b, ApJ, 276, 127
Jogee S., 2006, in Alloin D., ed., Lecture Notes in Physics, Berlin Springer Verlag Vol. 693, Physics of Active Galactic Nuclei at all Scales. p. 143 (arXiv:astro-ph/0408383), doi:10.1007/3-540-34621-X_6
Johansson P. H., Naab T., Burkert A., 2009, ApJ, 690, 802
Kalinova V., et al., 2017, MNRAS, 469, 2539
Katz N., Gunn J. E., 1991, ApJ, 377, 365
Kauffmann G., Haehnelt M., 2000, MNRAS, 311, 576
Kauffmann G., White S. D. M., Guiderdoni B., 1993, MNRAS, 264, 201
Kauffmann G., Colberg J. M., Diaferio A., White S. D. M., 1999, MNRAS, 303, 188
Kaufmann T., Mayer L., Wadsley J., Stadel J., Moore B., 2007, MNRAS, 375, 53
Kelvin L. S., et al., 2014, MNRAS, 444, 1647
Kent S. M., 1986, AJ, 91, 1301
Kent S. M., 1987, AJ, 93, 816
Kent S. M., 1988, AJ, 96, 514
Kereš D., Katz N., Weinberg D. H., Davé R., 2005, MNRAS, 363, 2
Kimm T., Devriendt J., Slyz A., Pichon C., Kassin S. A., Dubois Y., 2011, preprint, (arXiv:1106.0538)
Kormendy J., 1977, ApJ, 218, 333
Kormendy J., Cornell M. E., 2004, in Block D. L., Puerari I., Freeman K. C., Groess R., Block E. K., eds, Astrophysics and Space Science Library Vol. 319, Penetrating Bars Through Masks of Cosmic Dust. p. 261 (arXiv:astro-ph/0407434), doi:10.1007/978-1-4020-2862-5_24
Kormendy J., Gebhardt K., 2001, in Wheeler J. C., Martel H., eds, American Institute of Physics Conference Series Vol. 586, 20th Texas Symposium on relativistic astrophysics. pp 363–381 (arXiv:astro-ph/0105230), doi:10.1063/1.1419581
Kormendy J., Ho L. C., 2013, ARA&A, 51, 511
Kormendy J., Kennicutt Jr. R. C., 2004, ARA&A, 42, 603
Kormendy J., Bender R., Cornell M. E., 2011, Nature, 469, 374
Kravtsov A. V., 2003, ApJ, 590, L1
Krumholz M. R., Burkhart B., Forbes J. C., Crocker R. M., 2018, MNRAS,
Lacey C., Cole S., 1993, MNRAS, 262, 627
Lagos C. D. P., Cora S. A., Padilla N. D., 2008, MNRAS, 388, 587
Lange R., et al., 2015, MNRAS, 447, 2603
Laurikainen E., Salo H., Buta R., 2005, MNRAS, 362, 1319
Laurikainen E., Salo H., Buta R., Knapen J. H., Comerón S., 2010, MNRAS, 405, 1089
Le Fèvre O., et al., 2000, MNRAS, 311, 565
Liske J., et al., 2015, MNRAS, 452, 2087
Lotz J. M., et al., 2008, ApJ, 672, 177
Lynden-Bell D., Kalnajs A. J., 1972, MNRAS, 157, 1
Lynden-Bell D., Pringle J. E., 1974, MNRAS, 168, 603
MacArthur L. A., Courteau S., Holtzman J. A., 2003, ApJ, 582, 689
Magorrian J., et al., 1998, AJ, 115, 2285
Marconi A., Hunt L. K., 2003, ApJ, 589, L21
Martinez-Valpuesta I., Shlosman I., Heller C., 2006, ApJ, 637, 214
McConnell N. J., Ma C.-P., 2013, ApJ, 764, 184
McGaugh S. S., 2012, AJ, 143, 40
McGaugh S. S., Schombert J. M., Bothun G. D., de Blok W. J. G., 2000, ApJ, 533, L99
Méndez-Abreu J., Debattista V. P., Corsini E. M., Aguerri J. A. L., 2014, A&A, 572, A25
Mihos J. C., Hernquist L., 1994, ApJ, 425, L13
Mo H. J., Mao S., White S. D. M., 1998, MNRAS, 295, 319
Moffett A. J., et al., 2016, MNRAS, 457, 1308
Monaco P., Fontanot F., Taffoni G., 2007, MNRAS, 375, 1189
Nair P. B., Abraham R. G., 2010, ApJS, 186, 427
Navarro J. F., Steinmetz M., 1997, ApJ, 478, 13
Navarro J. F., Steinmetz M., 2000, ApJ, 528, 607
Navarro J. F., White S. D. M., 1993, MNRAS, 265, 271
Navarro J. F., White S. D. M., 1994, MNRAS, 267, 401
Navarro J. F., Frenk C. S., White S. D. M., 1995, MNRAS, 275, 56
Nowak N., Thomas J., Erwin P., Saglia R. P., Bender R., Davies R. I., 2010, MNRAS, 403, 646
Obreschkow D., Glazebrook K., 2014, ApJ, 784, 26
Ocvirk P., Pichon C., Teyssier R., 2008, MNRAS, 390, 1326
Peebles P. J. E., 1969, ApJ, 155, 393
Peebles P. J. E., 1984, ApJ, 277, 470
Peng C. Y., 2007, ApJ, 671, 1098
Pfenniger D., Norman C., 1990, ApJ, 363, 391
Porter L. A., Somerville R. S., Primack J. R., Johansson P. H., 2014, MNRAS, 444, 942
Posti L., Fraternali F., Di Teodoro E. M., Pezzulli G., 2018, A&A, 612, L6
Raha N., Sellwood J. A., James R. A., Kahn F. D., 1991, Nature, 352, 411
Rees M. J., Ostriker J. P., 1977, MNRAS, 179, 541
Robertson B., Cox T. J., Hernquist L., Franx M., Hopkins P. F., Martini P., Springel V., 2006a, ApJ, 641, 21
Robertson B., Bullock J. S., Cox T. J., Di Matteo T., Hernquist L., Springel V., Yoshida N., 2006b, ApJ, 645, 986
Romanowsky A. J., Fall S. M., 2012, ApJS, 203, 17
Romeo A. B., Falstad N., 2013, MNRAS, 433, 1389
Romeo A. B., Fathi K., 2016, MNRAS, 460, 2360
Sachdeva S., Saha K., 2018, preprint, (arXiv:1804.10072)
Saha K., Cortesi A., 2018, preprint, (arXiv:1807.02986)
Sani E., Marconi A., Hunt L. K., Risaliti G., 2011, MNRAS, 413, 1479
Scarlata C., et al., 2004, AJ, 128, 1124
Sellwood J. A., 2014, Reviews of Modern Physics, 86, 1
Sersic J. L., 1968, Atlas de Galaxias Australes
Shankar F., Marulli F., Bernardi M., Dai X., Hyde J. B., Sheth R. K., 2010, MNRAS, 403, 117

Shankar F., Marulli F., Mathur S., Bernardi M., Bournaud F., 2012, A&A, 540, A23
Shankar F., Marulli F., Bernardi M., Mei S., Meert A., Vikram V., 2013, MNRAS, 428, 109
Shankar F., et al., 2016, MNRAS, 460, 3119
Shen S., Mo H. J., White S. D. M., Blanton M. R., Kauffmann G., Voges W., Brinkmann J., Csabai I., 2003, MNRAS, 343, 978
Silk J., 1977, ApJ, 211, 638
Somerville R. S., Primack J. R., 1999, MNRAS, 310, 1087
Somerville R. S., Primack J. R., Faber S. M., 2000, ArXiv Astrophysics e-prints,
Somerville R. S., Hopkins P. F., Cox T. J., Robertson B. E., Hernquist L., 2008, MNRAS, 391, 481
Springel V., 2005, MNRAS, 364, 1105
Springel V., Yoshida N., White S. D. M., 2001, New Astron., 6, 79
Springel V., et al., 2005, Nature, 435, 629
Stark D. V., McGaugh S. S., Swaters R. A., 2009, AJ, 138, 392
Stevens A. R. H., Lagos C. d. P., Contreras S., Croton D. J., Padilla N. D., Schaller M., Schaye J., Theuns T., 2017, MNRAS, 467, 2066
Stewart K. R., Bullock J. S., Wechsler R. H., Maller A. H., 2009, ApJ, 702, 307
Sweet S. M., Fisher D., Glazebrook K., Obreschkow D., Lagos C., Wang L., 2018, ApJ, 860, 37
Tissera P. B., White S. D. M., Pedrosa S., Scannapieco C., 2010, MNRAS, 406, 922
Tonini C., Mutch S. J., Croton D. J., Wyithe J. S. B., 2016, MNRAS, 459, 4109
Toomre A., 1964, ApJ, 139, 1217
Toomre A., Toomre J., 1972, ApJ, 178, 623
Torres-Flores S., Epinat B., Amram P., Plana H., Mendes de Oliveira C., 2011, MNRAS, 416, 1936
Trachternach C., de Blok W. J. G., McGaugh S. S., van der Hulst J. M., Dettmar R.-J., 2009, A&A, 505, 577
Tully R. B., Fisher J. R., 1977, A&A, 54, 661
Vaghmare K., Barway S., Kembhavi A., 2013, ApJ, 767, L33
Walter F., Brinks E., de Blok W. J. G., Bigiel F., Kennicutt Jr. R. C., Thornley M. D., Leroy A., 2008, AJ, 136, 2563
Weinzirl T., Jogee S., Khochfar S., Burkert A., Kormendy J., 2009, ApJ, 696, 411
White S. D. M., 1984, ApJ, 286, 38
White S. D. M., Frenk C. S., 1991, ApJ, 379, 52
White S. D. M., Rees M. J., 1978, MNRAS, 183, 341
Wilman D. J., Erwin P., 2012, ApJ, 746, 160
York D. G., et al., 2000, AJ, 120, 1579
Zavala J., Avila-Reese V., Hernández-Toledo H., Firmani C., 2003, A&A, 412, 633
Zavala J., Okamoto T., Frenk C. S., 2008, MNRAS, 387, 364
Zhang Y., Yang X., 2017, preprint, (arXiv:1707.04979)
de Vaucouleurs G., 1948, Annales d'Astrophysique, 11, 247
van Dokkum P. G., 2005, AJ, 130, 2647

APPENDIX A:

The behaviour of our data in Fig. 3, Fig. 5, Fig. 6 and Fig. 9 is strongly regulated by different fractions of angular momentum losses. The following plots show those results for different values of f and for the HWT15 data. We choose to use $f = 0.8$ throughout this work as it provides better agreement with the observational data.

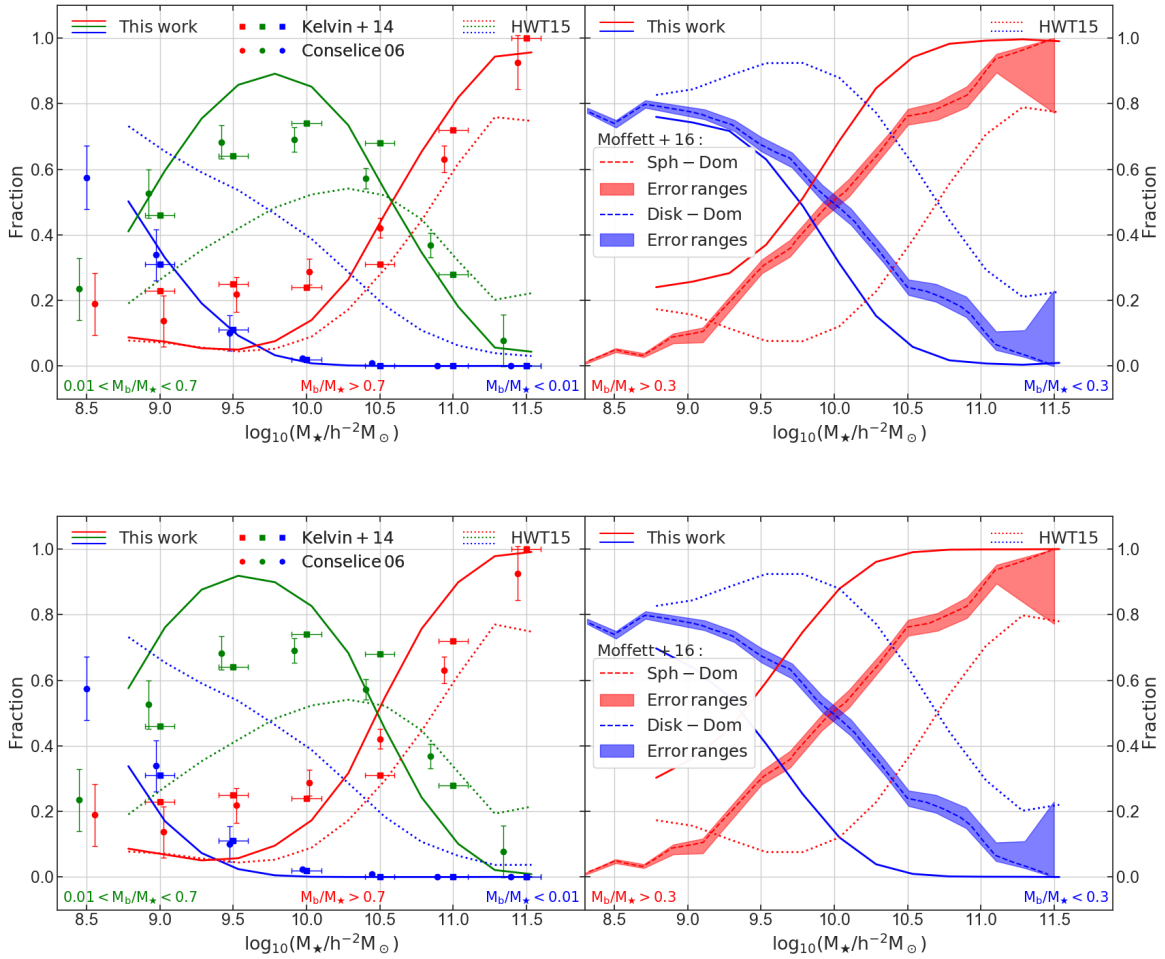

Figure A1. Same as Fig. 3. **Top panel:** f=0.6. **Bottom panel:** f=0.4.

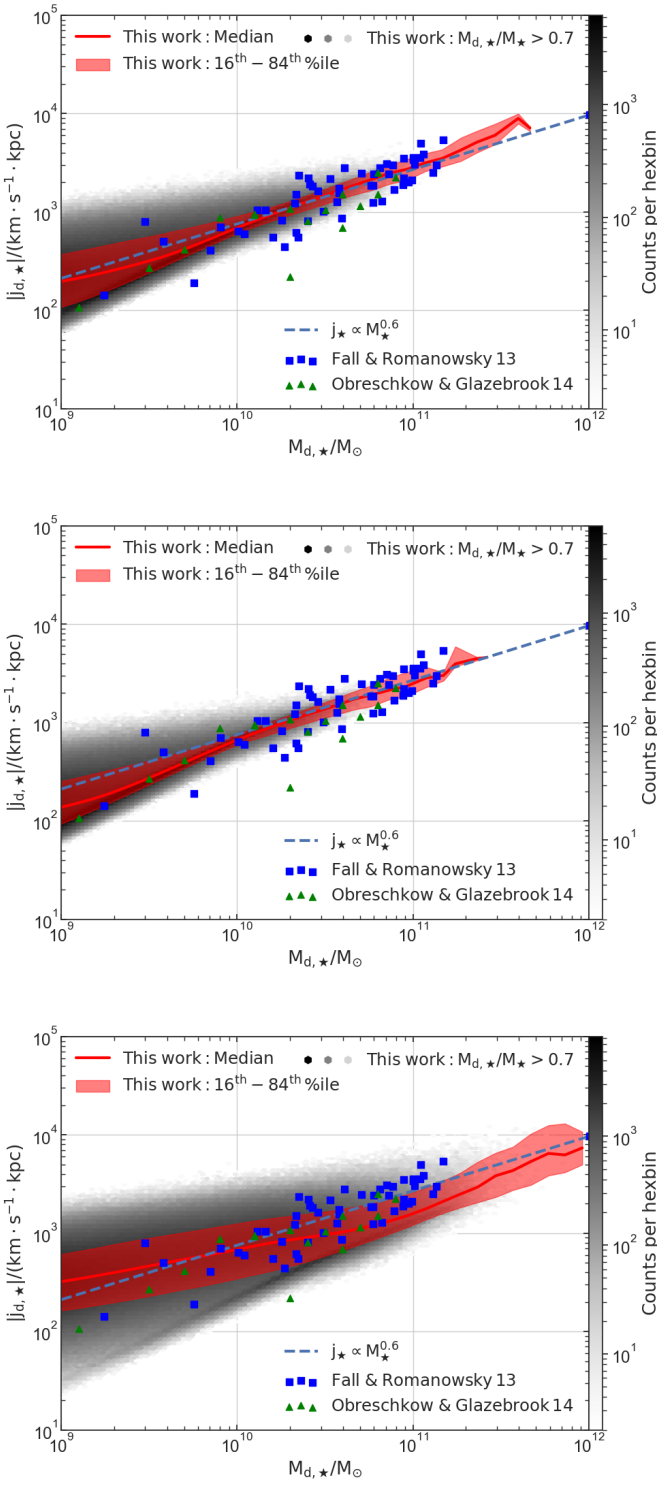

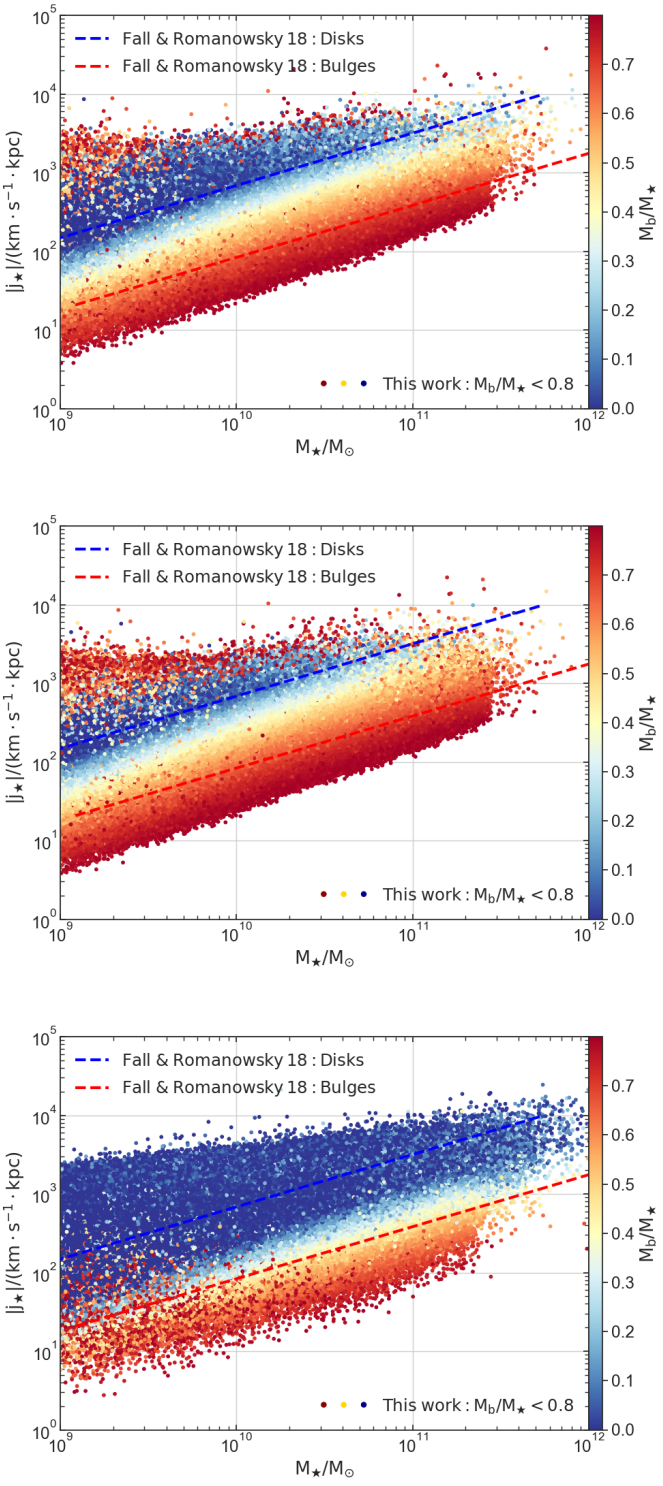

Figure A2. Same as Fig. 5. **Top panel:** f=0.6. **Middle panel:** f=0.4. **Bottom panel:** HWT15.

Figure A3. Same as Fig. 6. **Top panel:** f=0.6. **Middle panel:** f=0.4. **Bottom panel:** HWT15.

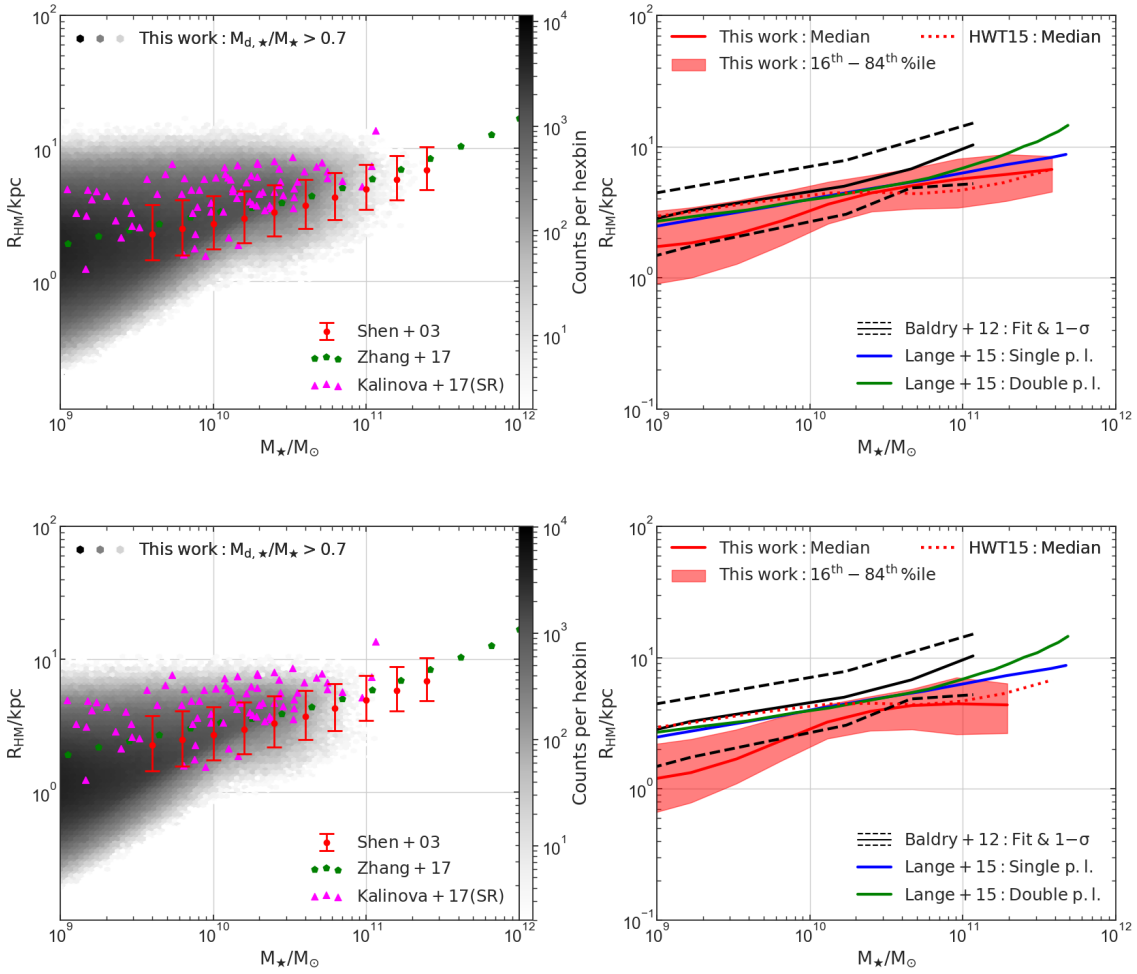

Figure A4. Same as Fig. 9. **Top panel:** f=0.6. **Middle panel:** f=0.4. **Bottom panel:** HWT15.